SCHWEIZ. MINERAL. PETROGR. MITT. 76, 453–474, 1996

# Geochronologic, petrologic and kinematic constraints on the evolution of the Err-Platta boundary, part of a fossil continent-ocean suture in the Alps (eastern Switzerland)

by *Mark R. Handy*[1], *Marco Herwegh*[2], *Balz S. Kamber*[3], *Reto Tietz*[2] and *Igor M. Villa*[3]

**Abstract**

The boundary between the Austroalpine Err nappe and the Penninic Platta unit represents part of a Late Cretaceous continent-ocean suture preserved in the highest stockwerk of the Tertiary Alpine orogen. Subduction and nappe stacking (D1) and subsequent extensional uplift (D2) along part of this suture are dated with the K–Ar method on two generations of syn-kinematic white mica in the Err nappe and with Ar–Ar step-heating of syn- to post-kinematic riebeckitic amphiboles in the Platta nappe. The first generation of white micas associated with isoclinal folds and W-directed mylonitic thrusting along nappe contacts yields a 76 to 89 Ma age range, whereas the second generation of white micas that grew during tight folding and top-to-the-E extensional D2 shearing yields 67 to 80 Ma ages. The K–Ar white mica ages are interpreted as ages of formation at the approximately 300 °C temperature of lower greenschist facies regional metamorphism in the southern part of the Err nappe. The two amphibole samples from the Platta nappe yield 69 and 73 Ma Ar–Ar ages, interpreted as syn-D2 formational ages. The Si-content of the white micas in chlorite-K-feldspar-quartz-bearing meta-radiolarites in the southern part of the Err nappe indicate a pressure decrease from D1 to D2 deformation, probably accompanied by an increase in temperature. This can be related to D2 extensional uplift accommodated along reactivated D1 nappe contacts in the footwall of the Julier-Bernina nappe. When combined with stratigraphic evidence, the radiometric ages and deformation-crystallization relations indicate clockwise P-T paths for the Err, Platta, and Margna nappes: Suturing of the Austroalpine continental and Liguro-Piemontese oceanic crust began with near surface thrusting and flysch sedimentation between 88 and 100 Ma and culminated with D1 folding and nappe stacking under high P/T greenschist facies conditions sometime during the period 80 to 88 Ma. The unroofing of this suture was a multi-stage process involving Late Cretaceous D2 extension under greenschist facies conditions, Early Tertiary D3 thrusting under lower anchizonal conditions, and mid-Tertiary D4 normal faulting above the uplifting Lepontine dome.

*Keywords:* nappe tectonics, metamorphism, continent-ocean suture, K–Ar method, Ar–Ar method, Penninic/Austroalpine boundary, Grisons, Switzerland.

## 1. Introduction and review of previous work

The boundary between Lower Austroalpine and Upper Penninic units in eastern Switzerland (Fig. 1) represents the suture between distal parts of the Apulian continental margin and the remains of the Jurassic Liguro-Piemontese or Tethyan oceanic crust in the Alps (e.g., TRÜMPY, 1975). In the detailed map of the study area in figure 2, the Apulian margin is represented by the Julier, Err, and Margna units, whereas the ophiolite-bearing Platta, Lizun and Forno units are considered to be relics of the Tethyan ocean. The mid- to late-Tertiary Engadine line (marked E in Fig. 1) offsets units that were continuous prior to faulting (e.g., the Err and Corvatsch nappes, the Julier and Bernina nappes, and the Lizun and Forno ophiolitic units). The Middle Penninic nappes to the west of the Turba mylonite zone (marked T in Fig. 1) are the structurally lowest units in the area and

[1] Institut für Geowissenschaften, Justus-Liebig-Universität, Senckenbergstrasse 3, D-35390 Giessen, Germany.
[2] Geologisches Institut, Universität Bern, Baltzerstrasse 1, CH-3012 Bern, Switzerland.
[3] Mineralogisch-Petrographisches Institut, Isotopengeologie, Universität Bern, Erlachstrasse 9a, CH-3012 Bern, Switzerland. Corresponding author: M.R. Handy. E-mail: Mark.Handy@geo.uni-giessen.de.

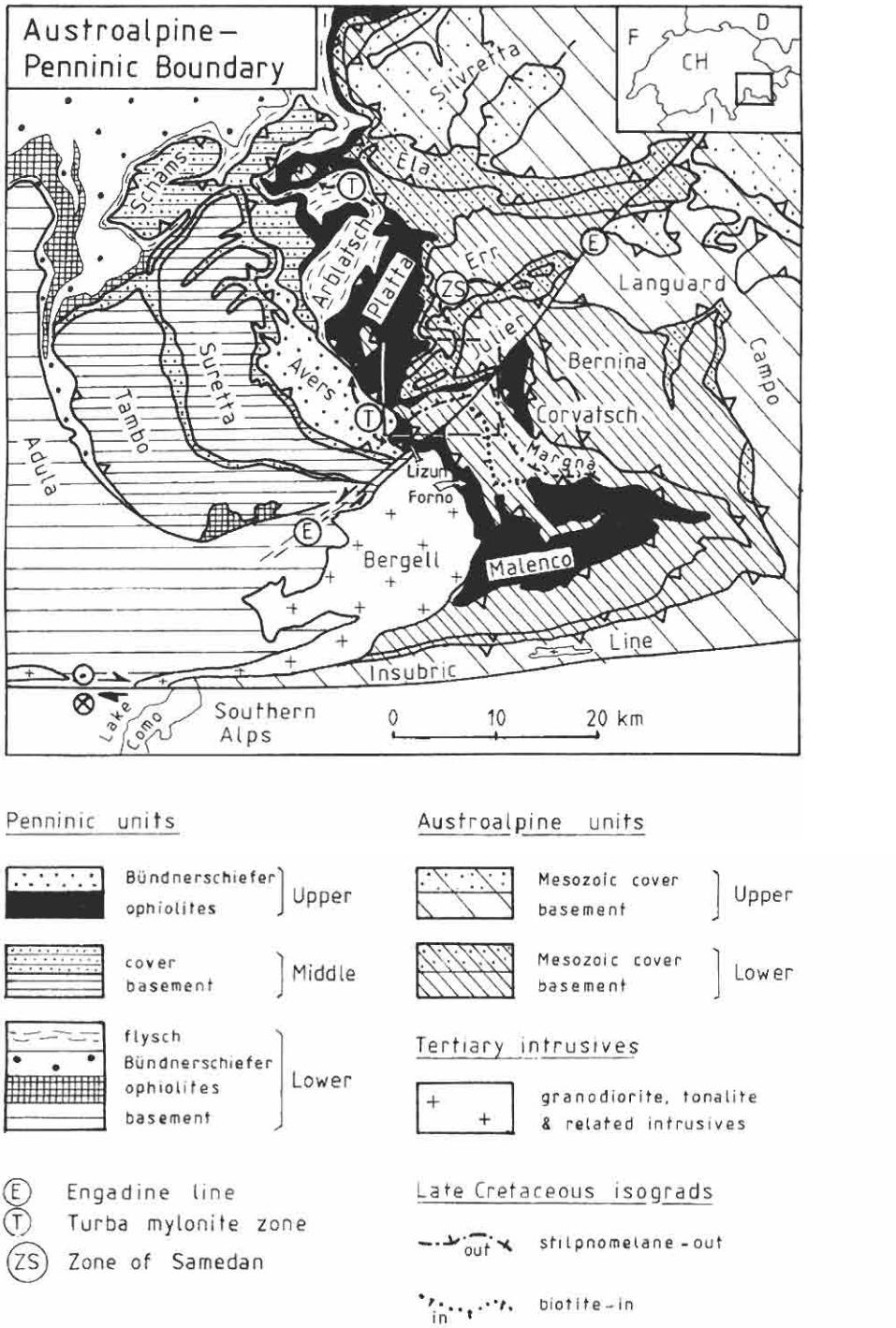


*Fig. 1* Overview of tectonic units at the transition from eastern to western Alps (adapted from Fig. 2 of HANDY, 1996). Boxed area in the center of the map indicates region depicted in greater detail in figure 2. Mineral isograds taken from TROMMSDORFF (1983) and LINIGER and GUNTLI (1988).

represent fragments of the distal European continental margin. They are treated only cursorily in this paper, but are the subject of other contributions in this volume. Differential erosion associated with mid- to late-Tertiary Lepontine doming centered to the west of the area in figure 1 is responsible for the exposure of progressively deeper levels of the nappe pile from east to west.

The tectonic history and paleogeography of the Lower Austroalpine and Upper Penninic units have been the source of speculation over the years, partly because the kinematics of deformation were not known until recently, but also due to the poor local constraints on the ages of the cover rocks and metamorphism. Both CORNELIUS (1932, 1950) and STAUB (1948) assumed Early Tertiary, N-directed thrusting and nappe stacking of the Austroalpine units (see Fig. 1 in HANDY et al., 1993), despite RÖSLI's (1945) discovery of Upper Cretaceous flysch at Murtiröl and beneath the Julier-Bernina thrust sheets in the Zone of Samedan (Fig. 1). Recent studies indicate that the imbrication of these units resulted primarily from W- to NW-directed thrusting and folding (LINIGER and NIEVERGELT, 1990) and subsequent extension during regional metamorphism, presumably in Late Cretaceous time (FROITZHEIM et al., 1994 and references therein). The sutured Lower Austroalpine and Upper Penninic units were then thrust as a coherent package at least 50 to 75 km northward onto the Early Tertiary Arblatsch flysch (Fig. 1; e.g., MILNES, 1978).

Regional metamorphic grade in the Austroalpine and South Penninic units in figure 1 increases from anchizonal conditions near Arosa in the north to biotite-greenschist facies in the Val Malenco in the south (TROMMSDORFF, 1983; FERREIRO MAHLMANN, 1995). In the northeastern part of the Zone of Samedan (marked ZS in Fig. 1), just north of the area discussed below, regional metamorphism attains upper anchizonal to epizonal conditions (FERREIRO MÄHLMANN, 1995). This regional metamorphism post-dates deposition of the youngest sediments in the Margna and Platta nappes (marly shales with planktonic foraminifera of Aptian-Albian, possibly Cenomanian age, DIETRICH, 1970), but pre-dates the middle Tertiary Bergell (Bregaglia) intrusion (TROMMSDORFF and NIEVERGELT, 1983).

Radiometric dating of minerals yields Late Cretaceous ages for the regional metamorphism described above. FREY et al. (1974) report Rb–Sr white mica and Rb–Sr and K–Ar biotite ages from the Margna nappe of between 60 and 80 Ma. The authors interpret the white mica ages as formational ages because the samples come from the Val Fex and Val Fedoz (Fig. 2), where mineral assemblages indicate temperatures of about 300 °C (LINIGER, 1992), well below the closure temperature of the Rb–Sr system in white mica. At these conditions, the biotite ages may be interpreted as cooling ages (see isograds and mineral compilation map in Fig. 8.4 of LINIGER, 1992), but FREY et al. (1974) do not specify whether the biotite-bearing samples were actually collected in the same area.

In the Platta nappe just northwest of the Engadine line (Figs 1 and 2), sodic to sodic-calcic amphiboles in Jurassic radiolarites grew syn- to post-kinematically with respect to the main schistosity and yield K–Ar ages ranging from 66 to 112 Ma (PHILLIP 1982; DEUTSCH, 1983). Neither of these authors characterize the main schistosity, although LINIGER (1992) claims that it formed during W-directed mylonitic thrusting under greenschist facies conditions. Both compositionally zoned and unzoned amphiboles were dated: Zoned amphiboles with actinolitic cores and riebeckitic rims yield the highest ages of 111.7 ± 2.0 Ma, whereas samples with the opposite zonation yield 90.2 ± 1.9 Ma ages. Mg-riebeckites from the same locality range in age from 66.5 ± 1.1 to 84.2 ± 1.3 Ma. DEUTSCH (1983) argues that the actinolitic cores of some amphiboles represent relics of oceanic metamorphism, whereas the rims grew later during Alpine metamorphism. A relatively young richterite age of 62 Ma is probably not relevant due to the presence of stilpnomelane inclusions in the richterite. DEUTSCH (1983) showed that stilpnomelane from the Platta nappe yields inconsistent, geologically meaningless ages. The wide spread of the amphibole ages may reflect excess Ar, which is known to be common in metamorphic amphiboles (VON BLANCKENBURG and VILLA, 1988) and is expected to be even more pronounced in K-poor amphiboles such as actinolite and riebeckite. As is evident from our own data below, an unequivocal geological interpretation of amphibole ages is seldom, and only a posteriori, possible.

Several other factors hinder a tectonic interpretation of these mineral ages: First, it is not clear which structures were actually dated. The ages were derived before workers reached a consensus that at least five kinematically distinct deformational phases affect the area (FROITZHEIM et al., 1994 and references therein). The first three of these phases are associated with schistosities, each comprising white mica, biotite, or in some cases chlorite (LINIGER, 1992; HANDY et al., 1993 and below). Second, the ages all come from rocks in structurally deeper units of the nappe pile; the somewhat lower grade metamorphism in the southern parts of the Err-Corvatsch nappe and

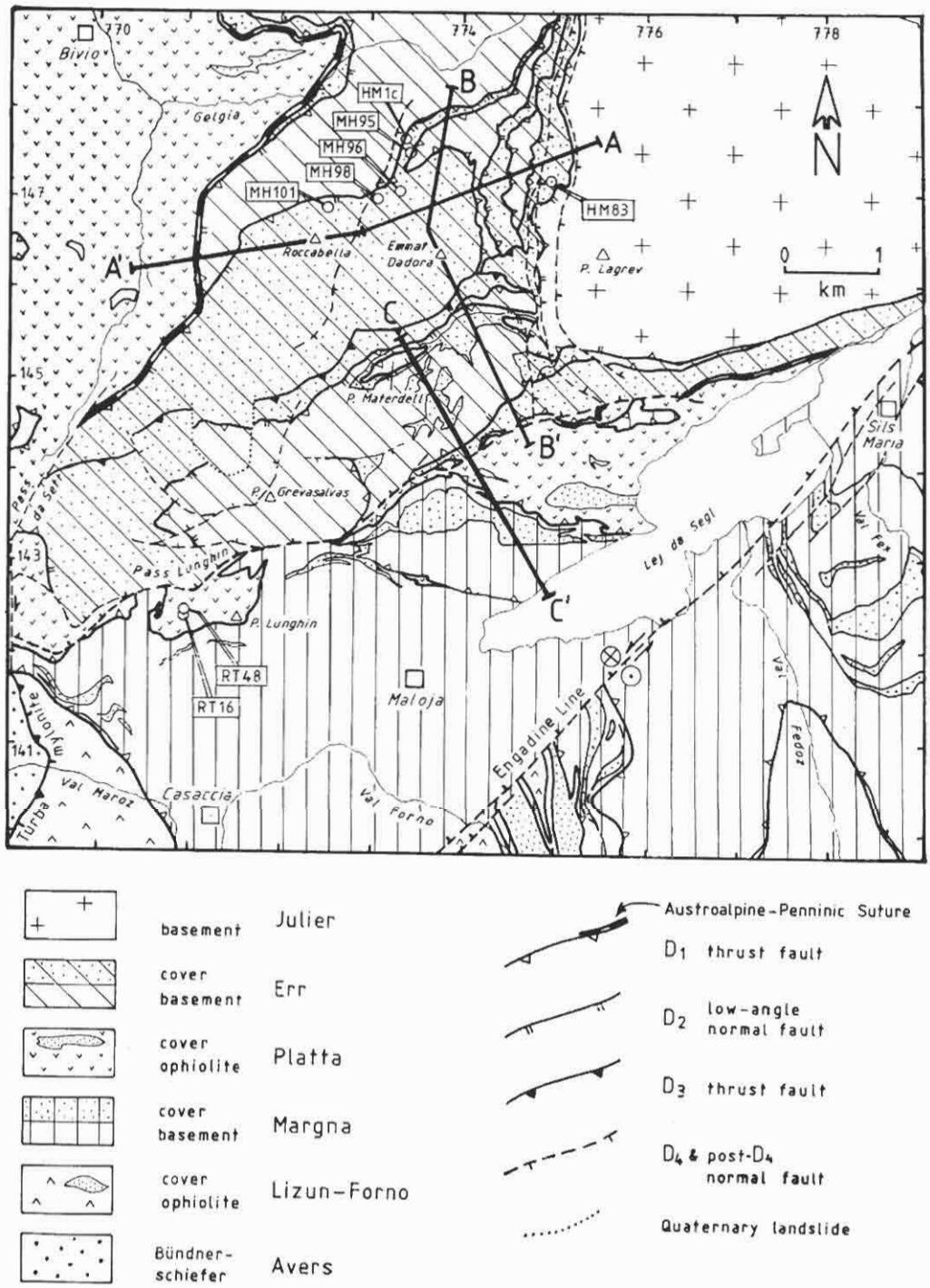


*Fig. 2* Tectonic map of the contact between Lower Austroalpine and Penninic units in the study area. Rectangles indicate numbers and locations of samples analyzed in this study. Lines correspond to traces of cross sections in figure 3. Swiss coordinate grid numbers indicated at the periphery of the map.

the Julier-Bernina nappe has not yet been dated. Finally, the physical conditions of regional metamorphism in these units are poorly constrained; better constraints are essential to interpreting mineral ages as formational or cooling ages.

In this paper, we readdress some of these problems and attempt to shed more light on the evolution of a part of the Austroalpine-Pennine suture at the junction between the eastern and western Alps. To this end, samples were collected for radiometric dating and geobarometric studies from the localities shown in figure 2. This area includes the Julier and Err nappes in the southern part of the Zone of Samedan (labelled ZS in Fig. 1), as well as parts of the Platta and Margna nappes mentioned above. Detailed mapping on the 1:10,000 scale conducted between 1990 and 1993 by M. Handy and five Diploma students (HERWEGH, 1992; REGLI, 1992; TIETZ, 1993; MATTENBERGER, 1994; KLAHR, 1994) provided a basis for establishing some of the key cross-cutting relationships between schistosities and relating these to large scale structures in the area (HANDY et al., 1993; HANDY, 1996). The first part of this paper therefore summarizes some of these relationships as a prelude to presenting new radiometric ages on syn-kinematic white mica and amphibole from the Err and Platta nappes. These ages are then related to changes in the depth of burial as determined from geobarometry on the same white mica-bearing assemblages used for dating. Finally, the implications of these new data are discussed in the broader context of subduction, accretion, uplift and exhumation during Late Cretaceous and Tertiary tectonics along part of the Apulian continental margin.

At this point, we wish to mention briefly that below, we use the term "exhumation" to refer to the unearthing of rocks at the erosional surface and "uplift" to describe the raising up or elevation of a rock body away from the Earth's center or towards the geoid ("uplift of rocks" of ENGLAND and MOLNAR, 1990). These are close to the standard definitions for these terms given in any English dictionary, and we employ them despite the current tendency to redefine "exhumation" as a synonym for uplift of rocks with respect to the surface (ENGLAND and MOLNAR, 1990), and to use "uplift" to refer to raising of the erosional surface ("surface uplift" of ENGLAND and MOLNAR, 1990).

## 2. Relationship of deformation to metamorphism

Three schistosity-forming, deformational phases can be distinguished in the Err nappe (HANDY et al., 1993) and in the underlying Platta and Margna units (LINIGER, 1992; HANDY, 1996): (i) D1 isoclinal folding and mylonitization under epizonal to greenschist facies conditions (FERREIRO MÄHLMANN, 1995); (ii) D2 close to tight folding and mylonitization, again under lower greenschist facies conditions; and (iii) D3 folding and thrusting under lower anchizonal conditions. High angle normal faulting associated with E–W extension (D4) along the Turba mylonite zone (Figs 1 and 2; LINIGER and NIEVERGELT, 1990; NIEVERGELT et al., 1996) and subsequent open folding (D5) occurred under brittle, lower anchizonal to unmetamorphic conditions in the study area (HANDY et al., 1993). The latter two phases are not considered here, but will be discussed again briefly in the final section. All of these deformational phases can be identified regionally in the Lower Austroalpine units, as summarized in FROITZHEIM et al. (1994). These authors have named D1, D2, and D3 in the Austroalpine units, respectively, the "Trupchun", "Ducan-Ela", and "Blaisun" phases.

The geologic cross sections in figure 3 depict the large-scale structures along the three section traces in figure 2. F1 and F2 folds have gently S-plunging axes and E-dipping axial planes in the eastern part of section A–A', but locally swing into an orientation with gently SW-plunging axes and SE-dipping axial planes in the western half of this section in the vicinity of the mountain peak labelled "Roccabella". In contrast, F3 folds have gently to moderately ESE-plunging axes with steeply dipping axial planes throughout the area (HANDY et al., 1993; HANDY, 1996). The Lunghin fault in sections B–B' and C–C' of figure 3 is a late (syn- to post-D4) oblique normal fault that juxtaposes the Err and Julier nappes in its hangingwall with the structurally deeper Platta and Margna nappes in its footwall.

The kinematics of the D1, D2, and D3 events differ markedly, as summarized in HANDY (1996). The shape preferred orientation of dynamically recrystallized quartz aggregates and the asymmetry of the quartz c-axis patterns in D1 mylonites (Fig. 4a) are consistent with top-to-the-W to -WSW noncoaxial shearing during D1. The S1 schistosity is penetrative in all units underlying the Julier nappe in figure 2. In contrast, D2 shearing is localized along D1 nappe contacts and the obliquity of D2 quartz c-axis patterns and grain shape orientations is not as pronounced as in D1 microfabrics (compare microstructures in Figs 4a and 4b). Slightly asymmetrical cross-girdle D2 quartz c-axis patterns suggest that top-to-the-E shearing included a strong component of flattening (Fig. 4b). This is consistent with FROITZHEIM's (1992) interpretation that the F2 folds formed

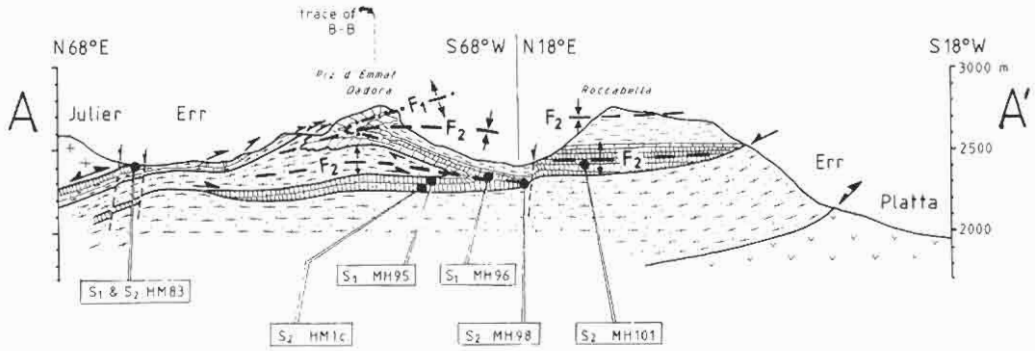


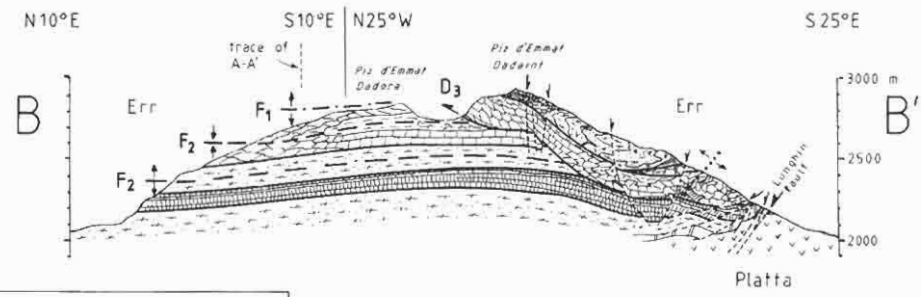


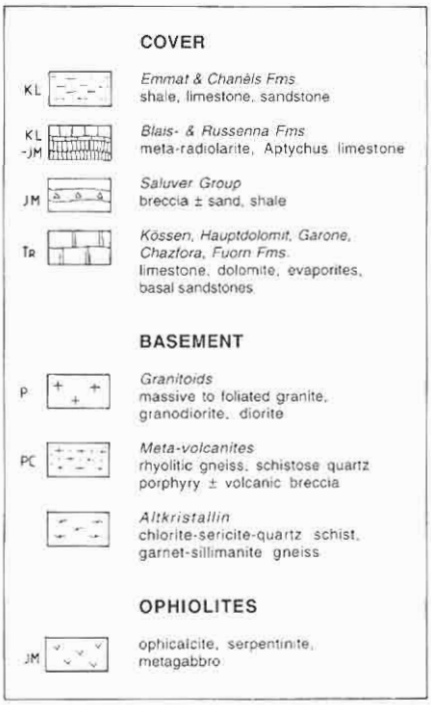


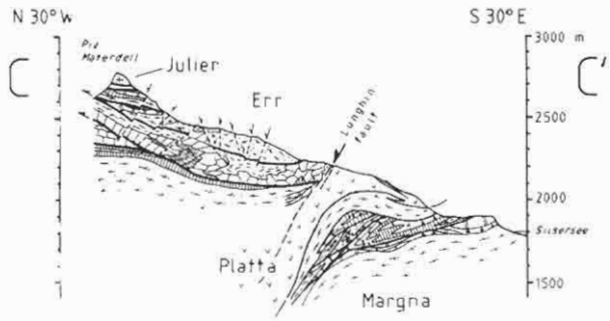


*Fig. 3* Geologic cross sections corresponding to traces in figure 2. A–A' shows major D1 and D2 structures. B–B' and C–C' show D3 structures and Lunghin fault. Cross sections synthesized from HERWEGH (1992), HANDY et al. (1993), MATTENBERGER (1994), and KLAHR (1994).

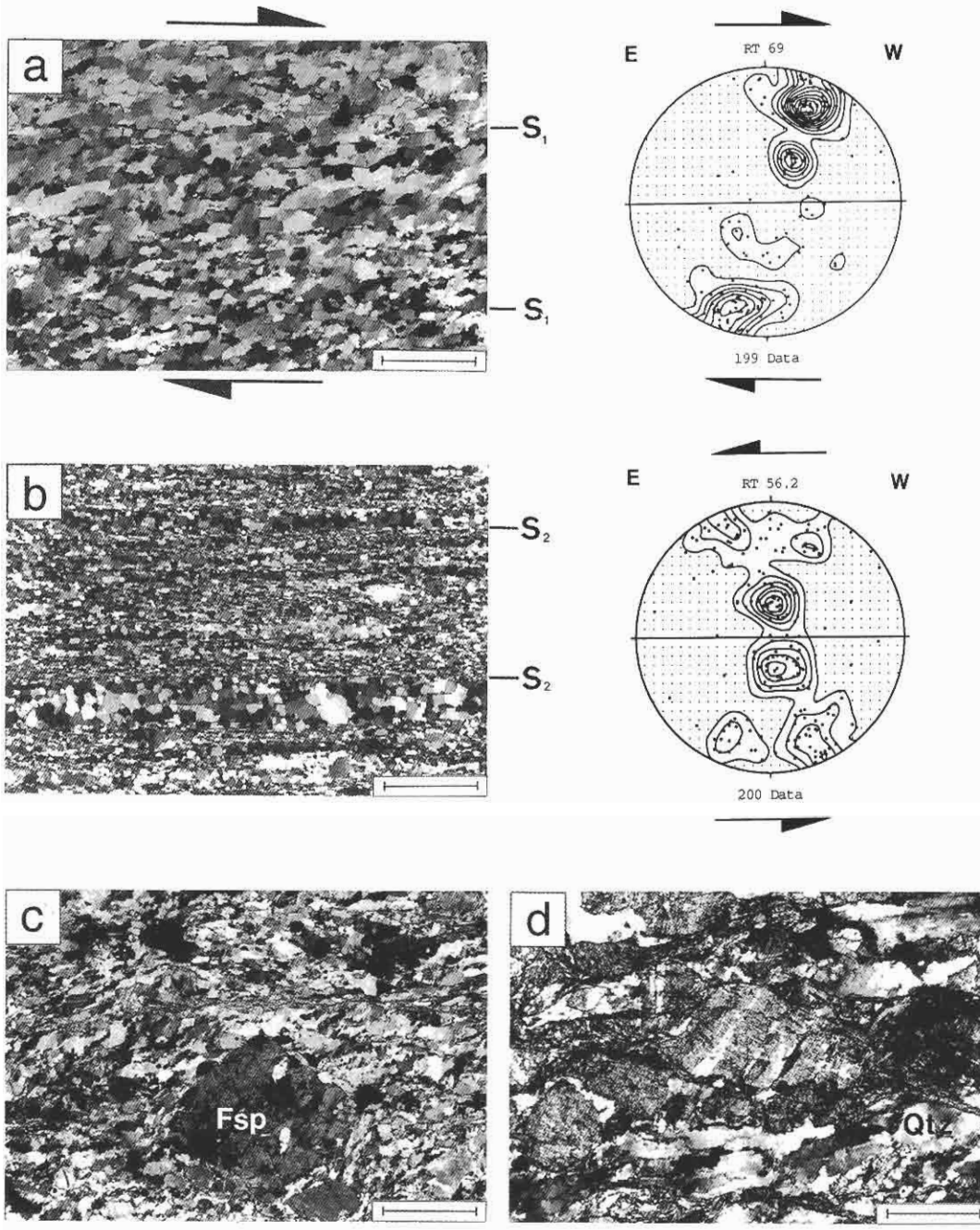


*Fig. 4* Microfabrics: (a) S1 quartz microstructure and c-axis pattern in Lower Triassic quartzite of the Margna nappe (sample RT69, coord. 771'680/142'980); (b) S2 quartz microstructure and c-axis pattern in Lower Triassic quartzite of the Margna nappe (sample RT56.2, coord. 770'700/142'260); (c) S1 quartz and feldspar (Fsp) microstructure in Maloja gneiss of the Margna nappe (sample RT59.2, coord. 699'270/141'790); (d) S2 quartz (Qtz) and feldspar microstructure from foliated granitoid rock at the base of the Julier nappe. Arrow shows quartz filling fractures in feldspar clast (sample HM25, coord. 775'300/149'140). Samples cut normal to foliation and parallel to lineation. Scale bar in all pictures is 1 mm.

*Tab. 1* Relationship between crystallization and deformation in meta-granitoids of the Julier, Err, and Margna nappes (a) and in meta-radiolarites of the Err and Platta nappes (b) northwest of the Engadine Line. Meta-granitoids include the Neir porphyritic gneiss, Err (Grevasalvas) granite, Margna (Maloja) augengneiss, Julier granodiorite, and Julier diorite. Standard mineral abbreviations from KRETZ (1983).

**a) Meta-granitoids**

| Event | | Qtz | Kfs | Pl | Ab | Ms | Phe | Ser | Czo/Ep | Pmp | Chl | Stp | Act | Cal | Tur | Ttn |
|---|---|---|---|---|---|---|---|---|---|---|---|---|---|---|---|---|
| pre- | Alpine | x | x | x | | x | | | x<br>1b | | | | x<br>1a, 1b | x | x<br>1a | x |
| **D1** | syn- | x | | | x | | x<br>1b | x<br>1a, 2, 3 | x | ? x ?<br>2 | x<br>x | | | | | |
| | post- | x | | | | | x<br>1b | x<br>1a, 2, 3 | x<br>1a, 2, 3 | ? x ?<br>2 | | ? x ?<br>1b | | | | |
| **D2** | syn- | x | | | x | | | x<br>1a, 2, 3 | x<br>1a, 2, 3 | ? x ?<br>2 | x | x<br>1a | x | | x<br>1a | x |
| | post | x | | | | | | x<br>1a, 2, 3 | x<br>1a, 2, 3 | ? x ?<br>2 | | x<br>1a | | | | |
| **D3** | syn- | | | | | | | x | | | x | | | x | | |

1 Observed only in granites: (1a) Grevasalvas granite, (1b) Maloja augengneiss
2 Observed only in Julier granodiorite
3 Observed only in Julier diorite

**b) Meta-radiolarites**

| Event | | Qtz | Kfs | Ab | Phe | Chl | Stp | Rbk | Act | Agt | Grt | Cal | Ttn |
|---|---|---|---|---|---|---|---|---|---|---|---|---|---|
| pre- | Alpine | x | x 2 | x | | | | | x 2 | | | x | x |
| **D1** | syn- | x | | x | x | x | | x 2 | | | | x | x |
| | post- | x | | | | | ? x 2 ? | | | ? x 2 ? | | x | |
| **D2** | syn- | x | | x | x | x | x 2 | x 2 | x 2 | | | x | |
| | post- | x | | | | x | x 2 | x 2 | x 2 | x 2 | x 2 | x | |
| **D3** | syn- | | | | | | | | | | | x | |

1 Observed only in the Err nappe
2 Observed only in the Platta nappe

during vertical shortening of an originally steeper dipping S1 schistosity. Nevertheless, the drag sense of S2 along reactivated D1 nappe contacts (e.g., section A–A' in Fig. 3) indicates that D2 shearing is locally very noncoaxial. Noncoaxial D2 shearing is pervasive in the footwall of the Julier nappe, along the base of the Err nappe and within the top of the Platta nappe. D3 accommodated N- to NNE-directed thrusting, as shown by the S-dipping ramps and northward displaced nappe contacts in section B–B' of figure 3. However, DÜRR (1992) observes the opposite thrusting sense (viz., to the S) in the Piz Neir area just north of the Gelgia valley. HANDY et al. (1993) propose that D3 thrusting and F3 folding manifest NNE–SSW shortening in the hangingwall of the major thrust transporting the Lower Austroalpine nappes and Upper Penninic ophiolite units northwards onto the Early Tertiary Arblatsch flysch (see discussion below in section V).

A problem in determining the relative age of deformation and mineral growth is that S1 and S2 mylonitic foliations are virtually indistinguishable due to their similar orientations and greenschist facies mineral assemblages. Differentiating these two foliations is particularly difficult in the Platta nappe and along the base of the Err nappe, where the S2 mylonitic foliation is locally penetrative and nearly coplanar with the otherwise dominant S1 mylonitic foliation. S2 can only be distinguished from S1 where the two foliations are clearly discordant (e.g., along the axial planes of F2 folds, just outside the boundaries of D2 shear zones) or along reactivated D1 nappe contacts, where top-to-the E sense of shear indicators show that S2 completely overprinted S1.

Table 1 summarizes the deformation-crystallization relationships for deformed meta-granitoids and meta-radiolarites, as determined in thin section using the optical criteria of MISCH (1969)

and SPRY (1969) for pre-, syn-, and post-kinematic recrystallization. None of the mineral parageneses from the mapped area contains biotite (Tab. 1), suggesting that the area lies north of the biotite-in isograd in figure 1 as mapped by TROMMSDORFF (1983) and LINIGER and GUNTLI (1988). In meta-granitoids of the Margna nappe northwest of the Engadine line, sericite in the north yields to phengite in the south (MATTENBERGER, 1994, p. 137, his Figs 2.1., 2.2.), corroborating the general trend of increasing metamorphic grade with structural depth in the nappe pile above the Turba mylonite zone. Na-amphiboles in meta-radiolarites of the Platta nappe are inferred to have grown over a prolonged period, starting during D1 and extending to post-D2 (Tab. 1; TIETZ, 1993, p. 25, coord. 770.870/142.430 and samples measured below).

The D1 and/or D2 metamorphic grade was somewhat higher in the Margna and Platta nappes and basal parts of the Err nappe than in the overlying Julier nappe. This is suggested by several features:

(i) the D1 and D2 quartz microstructures from the Margna nappe show subgrain rotation and grain boundary migration recrystallization in quartz (Figs 4a, 4b). Feldspars remain stable during both mylonitic events (e.g., Fig. 4c). In contrast, quartz in D2 mylonites from the base of the Julier basement nappe comprises elongate grains (Fig. 4d) that are diagnostic of dislocation glide with only limited subgrain rotation recrystallization. The brittly deformed feldspar in these mylonites (Fig. 4d) altered syn-kinematically to white mica and clinozoisite;

(ii) white mica and quartz grain size within Upper Jurassic Aptychus limestone (Russenna Formation), meta-radiolarian chert (Blais radiolarite) and Lower Cretaceous sandy limestones and marls (Emmat Formation) is larger in the Platta and Margna nappes than in the Err nappe (comparative microstructures in Fig. 7.4., p. 111 of KLAHR, 1994; see also TIETZ, 1993 and MATTENBERGER, 1994);

(iii) illite from argillaceous layers within the aforementioned marls and radiolarian cherts has slightly lower average Kübler index values in the Platta and Margna units (average = 0.24° 2Θ, range = 0.21– 0.26° 2Θ) than in the structurally higher Err unit exposed just northwest of the Lunghin fault (average = 0.25° 2Θ, range = 0.22–0.28° 2Θ, Figs 2 and 3, pp. 116–117 in HERWEGH, 1992; Figs 4.2., 4.3. in TIETZ, 1993; Fig. 2.5., Tab. 2.4. in MATTENBERGER, 1994).

D3 occurred under much lower grade (lower anchizonal) conditions than D1 and D2, regardless of location with respect to the nappe contacts and the Lunghin fault. For example, fine grained albite is observed to have grown during both D1 and D2, but not during D3 (Tab. 1). Similarly, quartz underwent dynamic recovery and recrystallization during D1 and D2, but behaved brittly during D3. These observations suggest that the entire area underwent uplift and/or cooling prior to D3 (see discussion in the final section).

## 3. Radiometric ages

### 3.1. SAMPLE LOCATIONS AND DESCRIPTIONS

The five mica-bearing samples dated with the K–Ar method all come from argillaceous layers within the Upper Jurassic (Malm, Tithon) Blais meta-radiolarite of the Err nappe (sample locations in Figs 2 and 3, and in Tab. 2a). We chose to date this rock type for two main reasons: First, it preserves S1 and S2 schistosities, respectively, in the limbs and hinges of a large scale F2 fold (peak labelled "Piz d'Emmat Dadora" in section A–A' of Fig. 3). This is also seen on the small scale (Fig. 5), where S2 locally overprints the folded S1 schis-

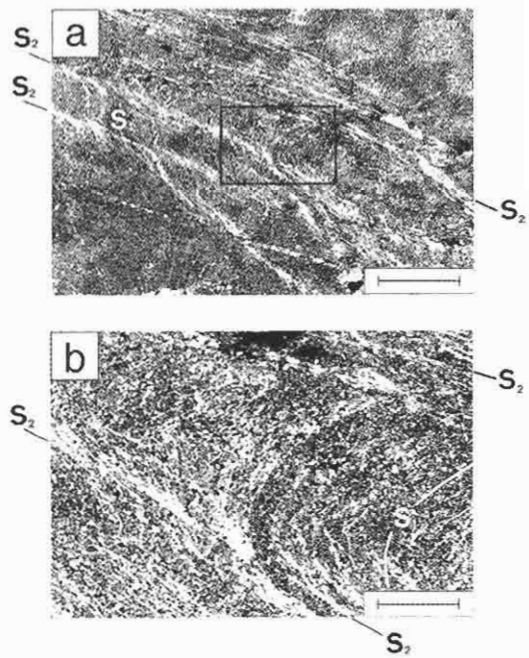


*Fig. 5* S1 and S2 schistosities in an F2 fold. (a) Overview showing S2 white micas forming the axial planar schistosity overprinting S1 white micas. Scale bar is 1 mm. (b) Detail of inset box in (a) showing S1–S2 relationship (sample HM83, coord. 774'950/148'150; location in Fig. 2, microprobe analyses in Tab. 3). Scale bar is 0.25 mm.

tosity in the hinge zone of F2. Second, of all the argillaceous lithologies in the Lower Austroalpine Mesozoic sequence, the Blais meta-radiolarite has the lowest volume proportion of detrital components. This minimizes the risk of measuring mica grains that might yield mixed ages.

The two riebeckite-bearing samples dated with the $^{40}Ar/^{39}Ar$ step-heating method come from mylonitic graphite-stilpnomelane-Na-amphibole-quartz-albite schist in the Platta nappe (CORNELIUS, 1950; sample locations in Fig. 2 and Tab. 2b). As mentioned above, PHILLIPP (1982) and DEUTSCH (1983) interpret this rock as a radiolarite that was metasomatically altered on the ocean floor in Jurassic time. In both of the measured samples (RT16 and RT48), most of the amphibole grains are riebeckitic, but some grains have actinolitic cores, as shown in figure 6. The amphibole grains in RT48 lie within both the S1 and S2 mylonitic foliation planes (Fig. 6 a) and show a weak alignment of their long axes parallel to the L2 stretching lineation. The presence of blue amphibole overgrowths in the pressure shadows of fractured grains aligned parallel to L2 (Fig. 6b) indicates that Na-amphibole grew during D2 shearing. In sample RT16 (Fig. 6c), most of the amphibole grains are oriented within S2, the only foliation observed in this particular sample. However, the possibility cannot be excluded that some of these preferentially oriented Na-amphiboles grew already during or after D1 shearing and underwent rotation and alignment into the S2 plane during D2 mylonitization. Numerous grains also grow across the foliation (cross-laths and rhombohedral grains in Figs 6 a, c). Taken together, these observations suggest that growth of the Na-amphiboles measured in this study occurred during both D1 and D2, and even outlasted D2.

The K/Ar white mica and $^{40}Ar/^{39}Ar$ amphibole results are summarized in tables 2a and 2b, respectively. Prior to the age analysis, the compositions of S1 and S2 white micas from sample HM83 and of riebeckitic amphiboles from samples RT-16 and RT-48 were analyzed with a Cameca SX-50 microprobe using an acceleration voltage of 15 kV and a 20 nA beam current. Complete analytical data for all the samples can be obtained directly from the authors.

### 3.2. K–Ar WHITE MICA AGES

The K/Ar analysis of white micas was performed with the extraction line described in FLISCH (1982), connected to a MM® 1200 mass spectrometer. Further details are given on p. 117 of TIETZ (1993).

Table 2a shows that the white mica grains oriented parallel to S1 yield an age range of 76 to 89 Ma, whereas S2 white micas parallel to the axial plane of F2 folds range in age from 67 to 80 Ma. This difference in age range corroborates microprobe analyses of S1 and S2 white micas from the small scale F2 fold in figure 5, indicating that the Si-content of S1 micas is consistently higher than that of S2 micas (see analyses in Tab. 3 and discussion below in section IV). As argon is not more mobile than major lattice-forming elements

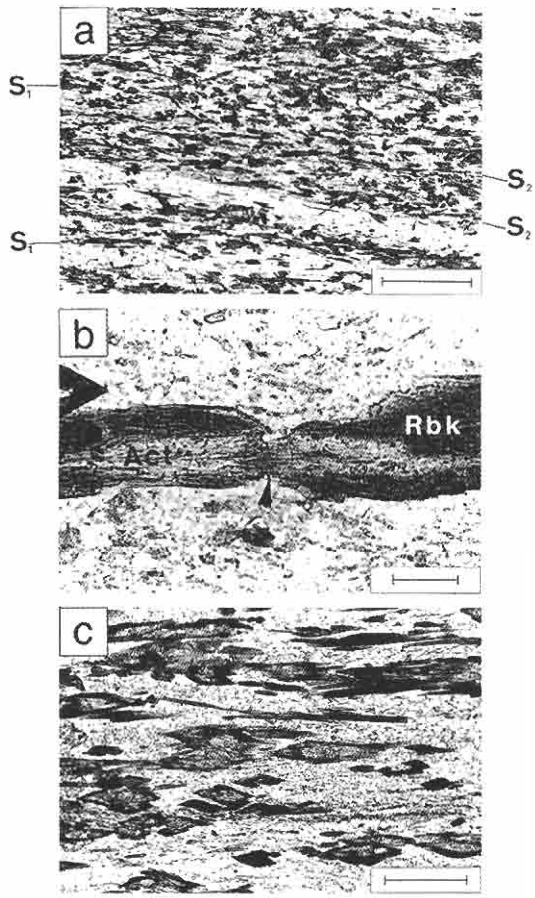


*Fig. 6* Microstructure in Na-amphibole schist from the Platta nappe: (a) Overview of sample RT48 with Na-amphibole defining S1 and S2 foliations. Scale bar is 1 mm. (b) Detail of (a) showing syn- to post-S2 growth of riebeckite (Rbk) on rims and in pressure shadow (arrow) of boudinaged actinolitic cores (Act). Scale bar is 0.25 mm. (c) Blue amphiboles from sample RT16 lying within the S2 foliation. Note rhombohedral grains oriented obliquely to L2. Scale bar is 0.05 mm. All sections cut normal to the S2 foliation and parallel to the L2 lineation.

*Tab. 2* K–Ar data from white micas in the Err nappe and summary of $^{40}Ar/^{39}Ar$ step-heating data from riebeckitic amphiboles in the Platta nappe.
(a) K % = potassium concentration in weight percent, $^{40}Ar^*$ = radiogenic $^{40}Ar$ concentration in nannoliters per gram (nl/g), $^{40}Ar^*$ % = percentage of radiogenic $^{40}Ar$ in total $^{40}Ar$.

| Sample | Rock | Structure | K % | $^{40}Ar^*$ nl/g | $^{40}Ar^*$ % | Age Ma | Coordinates of Sample location |
|---|---|---|---|---|---|---|---|
| MH 95 | meta-radiolarite | S1 | 1.7 | 5.1 | 81 | 76.1 ± 2.3 | 773'400/147'650 |
| MH 96 | meta-radiolarite | S1 | 1.3 | 4.5 | 75 | 89.1 ± 2.7 | 773'200/147'080 |
| MH 98 | meta-radiolarite | S2 | 2.4 | 6.4 | 71 | 67.5 ± 2.0 | 772'910/146'900 |
| MH 101 | meta-radiolarite | S2 | 2.0 | 6.1 | 72 | 79.7 ± 2.4 | 772'650/146'940 |
| HM 1c | meta-radiolarite | S2 | 3.6 | 9.9 | 67 | 70.3 ± 0.5 | 773'420/147'710 |

(b) Ar* (pl/g) is defined as total $^{40}Ar$ minus total $^{36}Ar$ x 295.5, following the usual convention. K, Cl and Ca concentrations were calculated from the reactor-produced Ar isotopes. Abbreviations: $t_{pl}$ = plateau age, $t_{is}$ = isochron age, n = number of steps used to calculate isochron, f = percent fraction of gas in these n steps, $Ar_i$ = trapped Ar composition, MSWD = scatter of isochron fit. All errors are 1σ.

| Sample | Rock | Structure | Ar ppm | K ppm | Cl ppm | Ca % | $t_{K/Ar}$ Ma | $t_{pl}$ Ma | n (f) | $t_{is}$ Ma | $Ar_i$ | MSWD | Coordinates of Sample location |
|---|---|---|---|---|---|---|---|---|---|---|---|---|---|
| RT 16 | K–Am schist | syn- to post-S2 | 375 | 837 | 2.2 | 1.8 | 112 | 72.4 ± 0.9 | 4 (85) | 75.0 ± 1.2 | 266 ± 22 | 1.9 | 770'970/142'410 |
| RT 48 | K–A schist | syn- to post-S2 | 250 | 933 | 1.5 | 1.7 | 68 | 68.2 ± 2.5 | 7 (84) | 69.4 ± 2.6 | 295 ± 19 | 1.9 | 770'970/142'420 |

(HAMMERSCHMIDT and FRANK, 1991), the age analyses and microprobe data both suggest that the S1 micas did not undergo any significant chemical or isotopic re-equilibration during D2 folding and shearing, even on the mm scale.

The K-content of the white mica in all samples is significantly less than the stoichiometric value of 9.8% (Tab. 2a), rendering a direct geologic interpretation of the ages apparently problematic. The low K values raise the question of whether the K–Ar system in white mica was open for K loss during post-D1 metamorphism, or whether white mica is merely intergrown with potassium-poor phases like quartz.

In order to answer this question, aliquots of the white mica separates used for radiometric age determinations were examined with the electron microprobe both in backscatter electron (BSE) imaging mode and by element mapping. The BSE images were used in combination with the element maps to identify impurities in the mineral separates: Fe was used to trace chlorite and opaques, Na to detect albite, and K to find white mica. Once impurities were located, their composition was determined by spot analysis in order to look for K-bearing phases other than white mica. Some representative results of the imaging are shown in figure 7.

It was found that the separated, measured grains actually comprise fine intergrowths on the ≤ 10 μm scale of phengitic muscovite, almost pure albite (Ab99), quartz, chlorite, and Fe ore. For example, the images for samples MH95 and MH96 in figure 7 reveal that the grains making up the S1 schistosity comprise muscovite (K map), chlorite (Fe map) and blasts of albite (Na map). Quartz (light areas in all the maps) makes up the matrix. Spot analysis of these impurities revealed that they are K-free. Similar element distribution patterns in the BSE images for sample MH101 (Fig. 7) indicate that the S2 schistosity also contains such intergrowths.

The BSE imaging suggests that the low K content of the white mica separates is a primary feature due to the dilution of the mucovite by syn-kinematically grown quartz, albite and chlorite, rather than to secondary alteration and K-depletion of muscovite. The K–Ar system in the white micas is therefore inferred to have remained undisturbed since its closure and so yields geologically interpretable ages. In light of the estimated 300 °C peak temperature of metamorphism in the area (FERREIRO MÄHLMANN, 1996), we interpret the S1 and S2 ages as formation ages that were not reset during later, lower grade deformation and metamorphism.

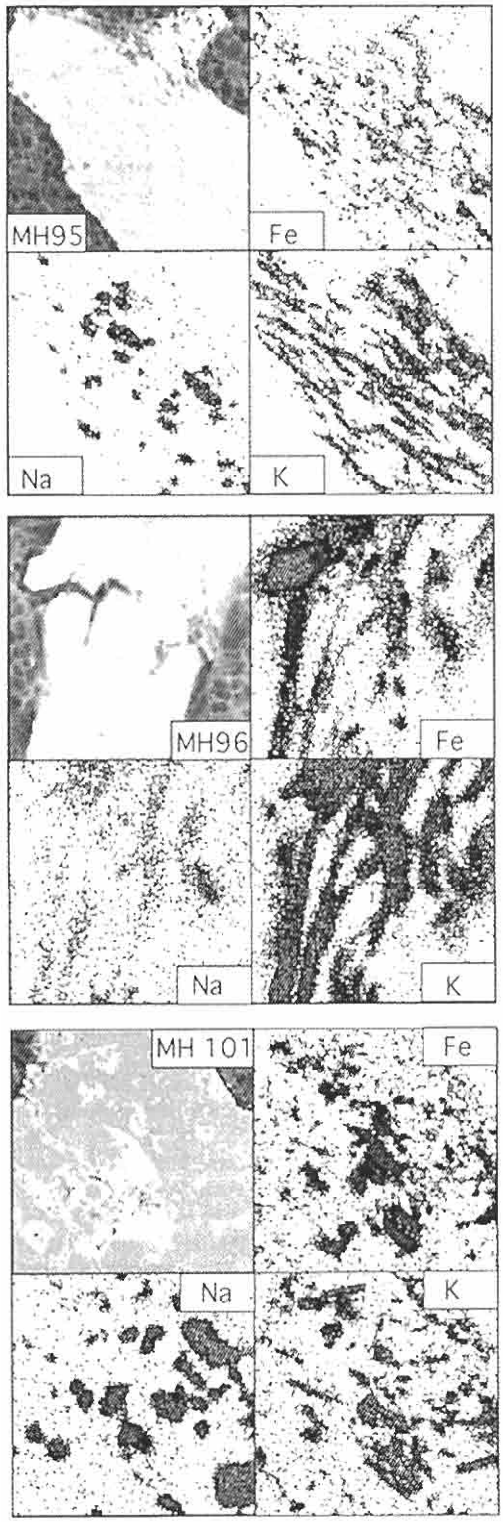


### 3.3. $^{40}Ar/^{39}Ar$ AMPHIBOLE AGES

Amphiboles from samples RT16 and RT48 were magnetically and gravimetrically sorted and then handpicked until a 100–150 μm size fraction was obtained. This was necessary to purify all samples sufficiently for radiometric measurement. The amphibole separates were irradiated in the TRIGA reactor in Pavia, Italy and analyzed in an all-metal extractions system connected to a MAP® 215-50B mass spectrometer.

The behaviour of the Ca-, Cl-, and K-derived isotopes listed in table 2b is the key to understanding the release pattern of the amphiboles in samples RT16 and RT48 shown in figure 8. As is usual for amphiboles with such complex microstructures and microscopic inclusions, both the Ca/K and Cl/K spectra display irregular variations (Figs 8 a, b). The constant Ca/K and very low Cl/K values in the middle portion of the release spectra probably pertain to the amphibole, whereas the steps at either end of the spectra may be attributed to Ca- and/or Cl-rich inclusions. Therefore, only the broad middle part of the age spectra in figure 8c contains information about the amphibole age. Although the middle parts of the plateaus and age spectra are not perfectly flat in either sample, their general uniformity indicates that they yield geologically meaningful ages.

Riebeckite in sample RT16 yields slightly higher isochron and plateau ages within the 1σ error than in sample RT48 (Tab. 2b). The plateau age of 72.4 Ma for RT16 is associated with a systematic uncertainty of 0.9 Ma due to nonideal behaviour. The plateau spans a large portion of the gas release (85%) and is characterized by Ca/K ratios that are only roughly constant (solid lines in Fig. 8a). This may reflect contamination of the riebeckite by one or more Ca-bearing phases having a similar Ar retention age to that of the host riebeckite. In contrast, riebeckite in sample RT48 has more irregular Ca/K and Cl/K spectra (dashed

*Fig. 7* Backscatter Electron (BSE) images and element maps of white mica separates (grain mounted aliquots) for the two S1 samples (MH95, MH96) and one S2 sample (MH101) used in the K–Ar age determinations. Within each set of images, the top left quadrant is a BSE picture, whereas the other three quadrants are element maps for iron (Fe), sodium (Na), and potassium (K) obtained by sweeping the electron beam over the defined area. Dark areas correspond to high element abundance. The apparent lack of shape preferred orientation in the images for MH101 reflects the fact that the mount surface is an oblique slice to the intergrown mica-rich aggregates. The width of each map is 80 μm (see text for explanation).

line in Figs 8 a, b) and yields a lower plateau age of 68.2 ± 2.5 Ma. The irregular spectra may reflect the preservation of both S1 and S2 Na-amphiboles in this sample (recall Fig. 6a).

There are two possible interpretations of these Na-amphibole ages that are consistent with the microstructural observations above:

(i) The 72.4 Ma age for RT16 could be interpreted as an S1 formation age, implying that most of the amphiboles formed during D1 and then rotated passively into the S2 foliation during D2 shearing. The younger age of RT48 reflects the coexistance of both S1 and S2 amphiboles, corroborating the irregular spectra mentioned above. Thus, the 68.2 Ma age of RT48 would represent a mixed S1–S2 age. A problem with this interpretation is that the D1 ages are much lower than the 76–89 Ma age range obtained from S1 white micas above.

(ii) The riebeckite ages from both samples are syn-D2 formation ages, with the higher age of RT16 attributed to a longer growth period of its amphiboles than for the amphiboles in RT48. This implies that the Ar budgets of both riebeckite samples are dominated by syn- to post-D2 growth. We prefer the latter interpretation because it accords better with the observed post-S2 growth of Na-amphibole and stilpnomelane (Tab. 1, cross-laths and rhombohedral grains in Fig. 6) and also explains the general coincidence of the age plateaus for the two samples (Fig. 8c).

Taken together, the white mica and riebeckite age data above allow us to draw conclusions of a more general nature, first about the behaviour of the K–Ar system in white mica, and second about the timing of D1 and D2. It is well known that white micas are rather unreliable chronometers at all grades of metamorphism. Illites from low grade rocks are reported to have been contaminated by non-rejuvenated detrital components as small as 2 μm (HUNZIKER et al., 1986, p. 176). Muscovites in medium grade gneisses frequently contain incompletely reset patches of phengite (HAMMERSCHMIDT and FRANK, 1991) that yield anomalously high ages. Moreover, white micas in eclogites are potential recipients of high pressure, excess Ar (TONARINI et al., 1993; LI et al., 1994). In our case, however, the overlap of the 67–80 Ma K–Ar white mica S2 age range with the syn-S2 69–73 Ma age range obtained from $^{40}Ar/^{39}Ar$ step-heating of riebeckites suggests that the white micas formed in an environment free of both detrital compositional influence and high pressure fluids carrying excess Ar. We therefore infer that the K–Ar ages on S1 and S2 white micas in our study reliably date D1 and D2 mylonitic shearing in the southern part of the Err nappe. A glance at table 2a, however, shows that the S1 and S2 white mica ages are not statistically different, especially given their fairly large variation outside the analytical uncertainty. This is particularly true for the younger of the two S1 ages (MH95), which falls within the range of S2 ages. It is not clear whether the large spread of S1 ages is real or apparent. Indeed, if MH95 was partly overgrown and reset during D2, it would obviously give an excessively low age and the correct age estimate of D1 would be closer to 89 Ma. Thus, the conservative statement is that not more than a few million years separated D1 nappe stacking and late orogenic D2 extension along the Lower Austroalpine-Penninic suture.

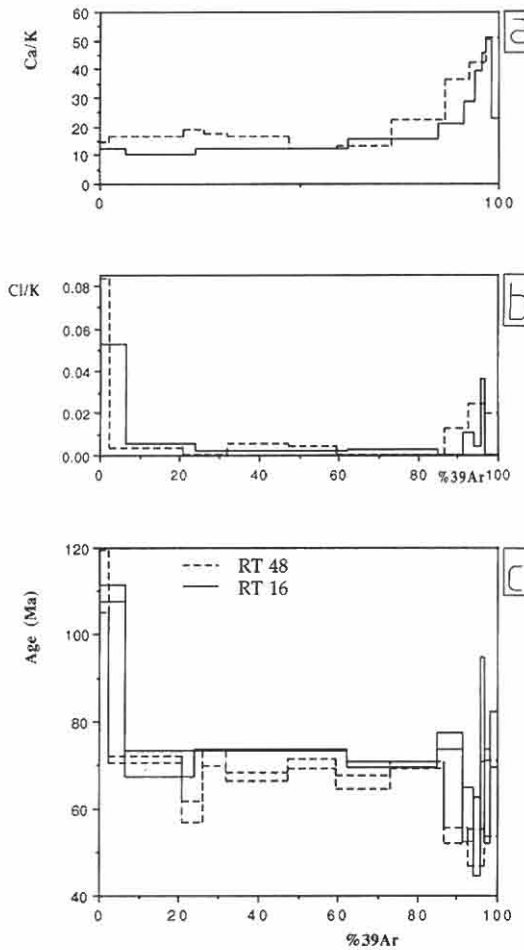


*Fig. 8* (a) Ca/K, (b) Cl/K and (c) Ar–Ar age spectra for blue amphiboles in samples RT16 and RT48 (see text for explanation).

*Tab. 3* Microprobe analyses of S1 and S2 white micas in sample HM83. Variations in the composition of S1 and S2 white micas may reflect the analysis of phases like quartz, chlorite or opaques that are intergrown with white mica on a scale comparable to that of the 1 μm spot size of the microprobe (see Fig. 7 and text for explanation).

| | S1 white micas (n = 17) | | | S2 white micas (n = 12) | | | recalculated |
|---|---|---|---|---|---|---|---|
| wt % | average | stdev | range | average | stdev | range | to lower $TiO_2$ |
| $SiO_2$ | 51.43 | 1.56 | 49.87–52.99 | 48.44 | 0.77 | 47.67–49.21 | 50.04 |
| $TiO_2$ | 0.33 | 0.25 | 0.08–0.58 | 3.29 | 1.10 | 2.19–4.39 | 0.25 |
| $Al_2O_3$ | 28.27 | 1.14 | 27.13–29.42 | 28.03 | 0.66 | 27.36–28.69 | 28.96 |
| FeO | 3.57 | 0.54 | 3.03–4.11 | 3.31 | 0.20 | 3.10–3.51 | 3.42 |
| MnO | 0.04 | 0.03 | 0.01–0.07 | 0.05 | 0.04 | 0.01–0.09 | 0.05 |
| MgO | 2.52 | 0.26 | 2.26–2.78 | 2.27 | 0.21 | 2.05–2.48 | 2.35 |
| CaO | 0.05 | 0.03 | 0.02–0.08 | 0.05 | 0.02 | 0.03–0.07 | 0.05 |
| $Na_2O$ | 0.25 | 0.19 | 0.06–0.44 | 0.15 | 0.03 | 0.12–0.18 | 0.18 |
| $K_2O$ | 8.57 | 0.75 | 7.82–9.33 | 9.20 | 0.21 | 8.99–9.40 | 9.50 |
| Cl | 0.03 | 0.03 | 0.00–0.06 | 0.04 | 0.02 | 0.01–0.06 | 0.06 |
| Total | 95.04 | 1.10 | 93.94–96.14 | 94.77 | 0.84 | 93.94–95.61 | 94.78 |
| Mineral formulas: atoms per 11.00 oxygens | | | | | | | |
| Si | 3.410 | 0.070 | | 3.256 | 0.034 | | 3.341 |
| Ti | 0.017 | 0.012 | | 0.167 | 0.055 | | 0.013 |
| Al | 2.210 | 0.092 | | 2.221 | 0.038 | | 2.280 |
| Fe | 0.198 | 0.031 | | 0.186 | 0.010 | | 0.191 |
| Mn | 0.003 | 0.002 | | 0.003 | 0.002 | | 0.003 |
| Mg | 0.249 | 0.025 | | 0.227 | 0.023 | | 0.232 |
| Ca | 0.003 | 0.002 | | 0.004 | 0.002 | | 0.004 |
| Na | 0.032 | 0.024 | | 0.020 | 0.004 | | 0.021 |
| K | 0.726 | 0.068 | | 0.789 | 0.022 | | 0.812 |

## 4. Phengite geobarometry and P-T conditions

Table 3 shows that white mica laths oriented parallel to S1 and S2 have different average compositions, particularly with respect to Si content: S1 and S2 micas average about 3.410 ± 0.070 and 3.256 ± 0.034 Si per formula unit, respectively. This difference in Si-content is partly attributable to the higher Ti-content of S2 micas (Tab. 3) and partly to the pressure-dependent Tschermak exchange in phengite ($Al_2(MSi)_{-1}$) according to the reaction (MASSONNE and SCHREYER, 1987):

3 celadonite = biotite + 4 K-feldspar + 6 quartz + $H_2O$

Although MASSONNE and SCHREYER (1987) calibrated this geobarometer for biotite-bearing assemblages, it can also be applied to assemblages with chlorite instead of biotite (as found in the study area). In this case, the Si content in white mica yields minimum pressures, according to the authors. Before using the white mica analyses to determine D1 and D2 pressures, we explored the possible causes of the anomalously high average $TiO_2$ values in the S2 micas (3.29 wt%, Tab. 3). The higher average Ti-content of the S2 micas may reflect substitution of Ti for Si on the white micas' octahedral sites or admixture of Ti-rich inclusions that are so small as to be unresolved by the 1 micron-size electron beam. To determine which possibility is more likely, we recalculated the composition of the S2 white micas. We assumed that the true Ti content of the S2 white micas is identical to that of the S1 white micas (0.33 wt% $TiO_2$) and then normalized the remaining oxides to the S2 total of 94.77 wt%. In this way, we hoped to recover the true S2 white mica composition (right-hand column of Tab. 3). Obviously, this procedure increases the concentrations of all non-Ti-bearing oxides relative both to the concentration of the putative inclusions and to the total wt% of S2 white mica. Recalculating the average S2 white mica composition reduces the difference of the average Si per formula unit (pfu) between S1 and S2 white micas by 52% (Tab. 3). Nevertheless, the Si pfu for S2 white micas is still significantly lower than that of the S1 white micas. Neither the original nor the recalculated average S2 compositions can be transformed to average S1 compositions by a simple Tschermak exchange. Using the recalculated S2 analysis, we could not match the shift in Al pfu with the shift in Si and $Me^{2+}$. On the other hand, using the original S2 analysis did not allow us to compensate the shift in Si and $Me^{2+}$ with Al.

Therefore, both explanations above for the high Ti content in S2 white micas are possible. Given that both Ti substitution and Ti impurities in S2 mica lowers its Si pfu relative to that of S1 mica, and because phengite geobarometry is subject to several uncertainties anyway (see discussion below), we decided to use the original compositional analysis to calculate the pressures.

When applied to the S1 and S2 white micas in this study, the phengite geobarometer yields a minimum pressure range of 800–900 MPa for D1 and 400–500 MPa for D2 at temperatures of 300 °C along the base of the Err nappe. At first appraisal, the D1 pressure range appears too high to be compatible with the greenschist facies mineral parageneses in the rocks. Indeed, it is generally conceded that the application of the phengite geobarometer to natural assemblages is fraught with problems. The synthetic phengite in the calibrating experiments of MASSONNE and SCHREYER (1987) had a disordered 1M structure rather than the ordered 2M or 3T structure that FREY et al. (1983) determined for the white micas of the study area. EVANS and PATRICK (1987) point out that this discrepancy between structural ordering of the micas in nature and in the calibrating experiments is the greatest weakness of the phengite geobarometer. In addition, MASSONNE and SCHREYER (1987) did not investigate the effect of substituting Ti for Si on the IV and VI coordination sites in the white mica lattice. As mentioned above, this substitution is suspected to be one of the causes of reduced Si content in S2 micas and may yield underestimates of the actual D2 pressure. Despite these unresolved problems, the pressures estimated with the phengite geobarometer may well be real. In a petrogenetic grid synthesizing recent petrological data, BOUSQUET et al. (in press, their Fig. 6) show that greenschist facies assemblages in a variety of rock types can remain stable to pressures as high as 800–900 MPa at the 300–350 °C temperatures estimated for regional metamorphism in the southern part of the Err nappe (see discussion below).

The P-T diagrams in figure 9 summarize our estimates of D1 and D2 conditions in the Err nappe (Fig. 9a) and LINIGER'S (1992) estimates of D1, D2, and D3 conditions in the Margna nappe southeast of the Engadine line (Figs 9 b, c). Based on the geobarometric data presented above, D1 mylonitization is believed to have occurred under high P/T greenschist facies conditions. This is consistent with the wide distribution of 3T-polytype white micas in the area (FREY et al., 1983), as well as the occurrence of blue amphiboles in rocks of the Margna and Platta nappes both northwest (CORNELIUS, 1932; PHILLIPP, 1982) and southeast of the Engadine line (GUNTLI and LINIGER, 1989; LINIGER, 1992). Due to the positive slope of the Si isopleths in figure 9, the decrease in Si content of

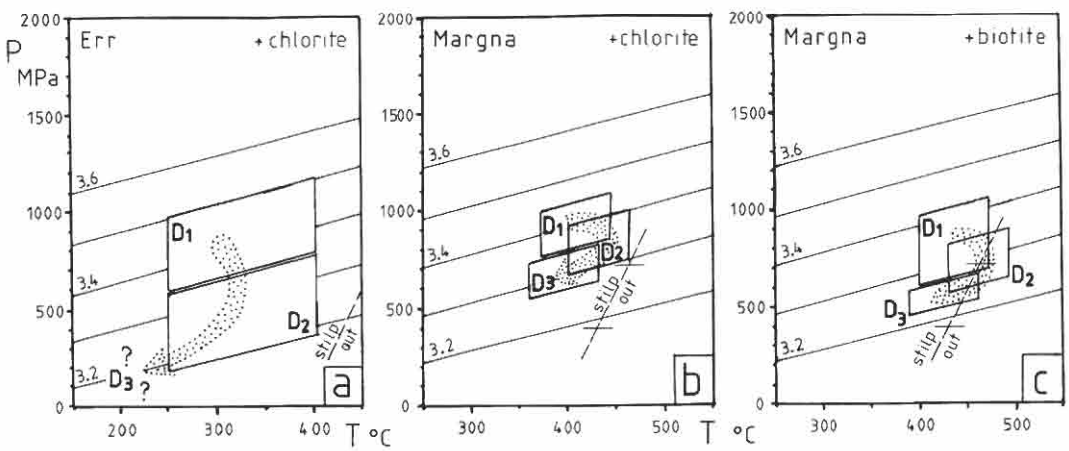


*Fig. 9* Pressure-Temperature (P-T) diagrams showing estimated conditions of metamorphism for (a) the base of the Err nappe, (b) part of the Margna nappe northwest of the biotite-in isograd in figure 1, (c) part of the Margna nappe south of the biotite-in isograd (b and c taken directly from Fig. 8.6 of LINIGER, 1992 for samples southeast of the Engadine line). Buffering phyllosilicate (chlorite or biotite) in the barometrically calibrated Si-exchange reaction of MASSONNE and SCHREYER (1987) is indicated in the upper right-hand corner of each diagram. Si-isopleths for white mica from MASSONNE and SCHREYER (1987). Stilpnomelane-out reaction curve (Stp + Phe => Bt + Chl + Qtz + $H_2O$) after NITSCH (1970). Stippled arrows indicate approximate P-T paths inferred from phengite geobarometer and other mineral assemblages (see text).

S2 micas with respect to S1 micas can be interpreted to reflect a pressure-decrease and/or a temperature-increase during D2. PHILLIPP (1982) points out that a temperature increase is necessary to explain the post-D2/pre-D3 growth of stilpnomelane and garnet (spessartine) in meta-radiolarite rocks of the Platta nappe. Unfortunately, temperatures during D1 and D2 in the Err nappe are poorly constrained; the post-D2 growth of stilpnomelane in meta-granitoids and -radiolarites (Tab. 1), the absence of staurolite in pelitic rocks, and the generally brittle behaviour of feldspar during both D1 and D2 (HANDY et al., 1993) all indicate temperatures less than 450–500 °C. FERREIRO MÄHLMANN (1996) deduces a maximum temperature of 300 °C from vitrinite reflectance and illite crystallinity values. A minimum temperature of about 250 °C during D1 and D2 in the Err nappe is estimated from the syn-kinematic growth of chlorite and white mica, and from the dynamic recrystallization of quartz.

Much lower temperatures of 150–250 °C are inferred for D3 in the southern part of the Err nappe from microstructural evidence of cataclasis with only limited crystal plasticity in quartz (i.e., undulose extinction, deformation bands), and from the dynamic recrystallization of calcite in limestones affected by D3 structures (HANDY et al., 1993). The pressure that prevailed in the Err nappe during D3 is unconstrained, but is certainly less than the D2 pressure values and probably also somewhat lower than LINIGER'S (1992) estimated D3 pressure range of 500 to 700 MPa for structurally deeper parts of the Margna nappe exposed southeast of the Engadine line (Figs 9 b, c). There, the rocks experienced a D3 temperature of about 400 °C (LINIGER, 1992). The 150–250 °C, 200–300 MPa contrast in D3 temperatures and pressures in the Err and Margna nappes (Fig. 9) is partly due to the difference in structural depth between these two units (ca. 4–5 km) and partly to mid- to late Tertiary, sinistral strike slip and differential block rotation along the Engadine line (Fig. 1). SCHMID and FROITZHEIM (1993) estimate that in the Maloja area, the southeastern side of the Engadine line (containing most of the Margna nappe) moved some 2.8 km northeastwards and was uplifted some 2.8 km with respect to the northwestern side.

The P-T conditions in the Platta ophiolites during D1 and D2 are very poorly constrained at present. However, the fact that the Platta nappe experienced the same sequence of deformation as the overlying Err nappe suggests that its P-T path has a similar clockwise shape to those of the adjacent Err and Margna nappes. The growth of blue amphibole during D1 and D2 indicates peak temperatures of at least 450 °C, a value which is not inconsistent with the close proximity of the Platta rocks in the area to the stilpnomelane-out isograd in the northern part of the Margna nappe (Fig. 1, see stability curve for stilpnomelane in Fig. 9). This temperature is significantly higher than the estimated D1 and D2 temperature (300–350 °C) in the Err nappe (see above) and may be attributed to the structural location of the Platta nappe in the hot footwall beneath the large D2 shear zone that accommodated extensional uplift along the Err-Platta boundary. This implies that the Platta nappe, and with it the structurally deeper Margna and Lizun-Forno units, were subducted to somewhat greater depths during D1 than the part of the Err nappe presently exposed.

To conclude this section, the Err, Platta, and Margna nappes are inferred to have clockwise P-T paths, but the absolute values of pressure and temperature along these paths vary somewhat with depth in the nappe pile and the buffering paragenesis (chlorite- vs biotite-bearing assemblages). Even if the minimum values of pressure derived from the phengite geobarometer are not trusted, however, the differences in pressures for D1, D2, and D3 in the various nappe units can be used to constrain their uplift history.

## 5. Correlation with events in adjacent units and tectonic implications

Numerous authors have already correlated the deformation history of the Lower Austroalpine units with events in adjacent units (nicely synthesized in FROITZHEIM et al., 1994, p. 593), so the discussion below is merely an attempt to integrate our new age and petrologic data into this framework and to discuss some of the implications of recently published structural and metamorphic work for the tectonothermal evolution of the area. Figure 10 relates the approximate P-T paths and radiometric ages for the Margna, Platta, and Err nappes to the tectonic evolution of the continent-ocean transition in the Lower Austroalpine and Penninic domains beginning in Early Mesozoic time, as depicted in a series of highly schematic cross sections (Figs 10a–g).

Early to Middle Jurassic rifting lead to the individuation of basins and highs in the Julier-Bernina, Err-Corvatsch, and Margna units (Fig. 10a; e.g., TRÜMPY, 1975; BERNOULLI et al., 1990). Early Mesozoic rifting features preserved in the Lower Austroalpine nappes are described in detail in EBERLI (1988); FROITZHEIM and EBERLI (1990); LINIGER (1992); SPILLMANN (1993); HANDY et al. (1993) and HANDY (1996). The configuration of

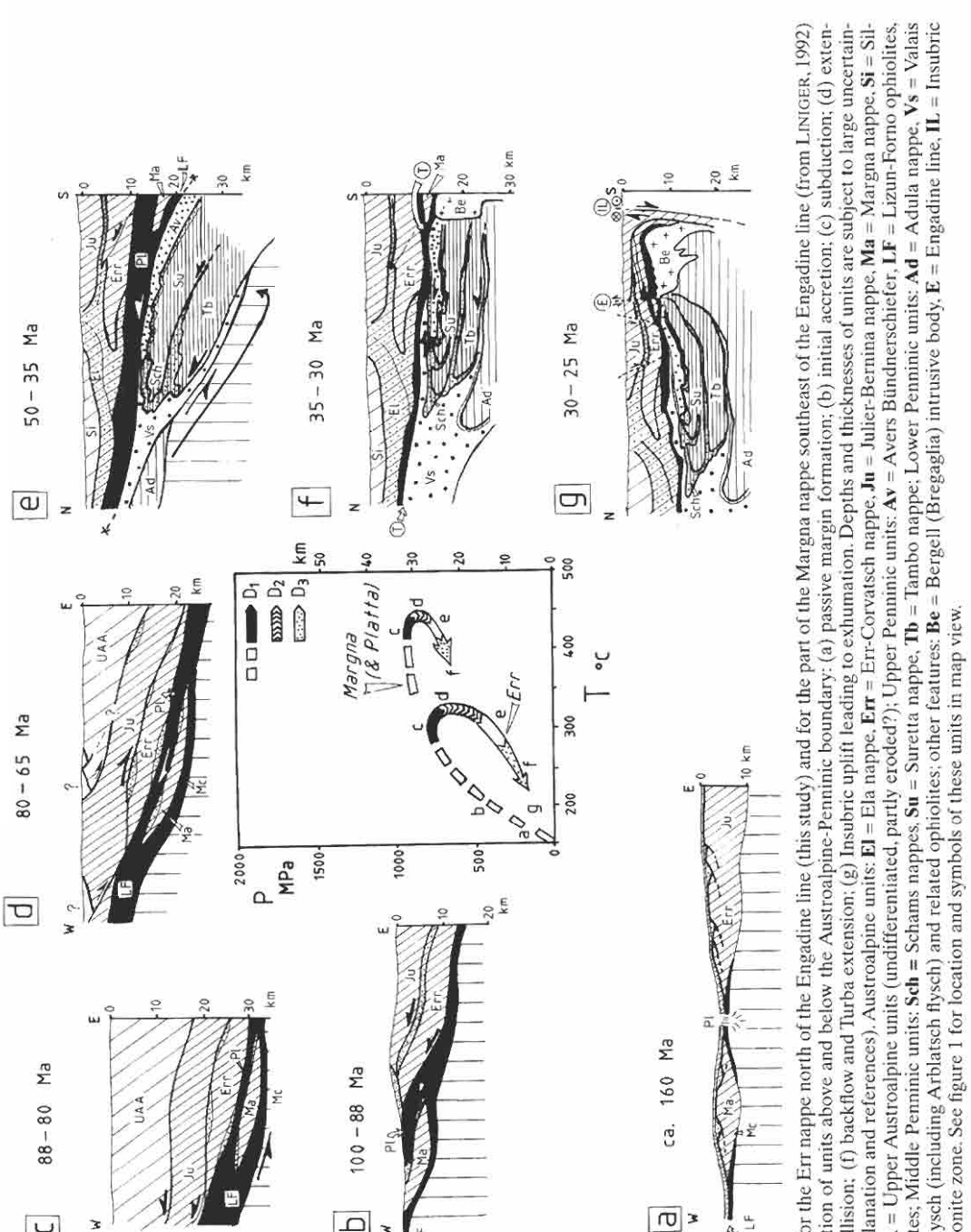


*Fig. 10:* P-T paths for the Err nappe north of the Engadine line (this study) and for the part of the Margna nappe southeast of the Engadine line (from LINIGER, 1992) and tectonic evolution of units above and below the Austroalpine-Penninic boundary: (a) passive margin formation; (b) initial accretion; (c) subduction; (d) extensional uplift; (e) collision; (f) backflow and Turba extension; (g) Insubric uplift leading to exhumation. Depths and thicknesses of units are subject to large uncertainty (see text for explanation and references). Austroalpine units: **El** = Ela nappe, **Err** = Err-Corvatsch nappe, **Ju** = Julier-Bernina nappe, **Ma** = Margna nappe, **Si** = Silvretta nappe, **UAA** = Upper Austroalpine units (undifferentiated, partly eroded?); Upper Penninic units: **Av** = Avers Bündnerschiefer, **LF** = Lizun-Forno ophiolites, **Pl** = Platta ophiolites; Middle Penninic units: **Sch** = Schams nappes, **Su** = Suretta nappe, **Tb** = Tambo nappe; Lower Penninic units: **Ad** = Adula nappe, **Vs** = Valais Bündnerschiefer, flysch (including Arblatsch flysch) and related ophiolites; other features: **Be** = Bergell (Bregaglia) intrusive body, **E** = Engadine line, **IL** = Insubric line, **T** = Turba mylonite zone. See figure 1 for location and symbols of these units in map view.

the passive margin affected the subsequent structural evolution of the Alpine edifice. The Margna nappe is inferred to have formed an extensional allochthon within the Liguro-Piemontese ocean (SPILLMANN, 1993; TIETZ, 1993; FROITZHEIM et al., 1994; HANDY, 1996) as a way of explaining its present location between remnants of this ocean (the Platta and Lizun-Forno units, Fig. 1). Stratigraphic similarities of the Margna cover with Err sediments of similar age (LINIGER and GUNTLI, 1988) indicate that the Margna nappe probably derived from the Apulian rather than the European margin (LINIGER, 1992). Drawing an analogy with the present day Ligurian margin, TROMMSDORFF et al. (1993) interpret the Malenco ultramafics and mafics as a small patch of partly altered upper mantle and lower crust that was extensionally uplifted from beneath intermediate levels of the Apulian continental crust in Early Mesozoic time.

Figure 10b depicts the onset of continent-ocean suturing. In this area, suturing involved W-directed subduction and accretion of the Lizun-Forno, Platta and Margna units to the distal parts of the Apulian margin, represented by the Err nappe. Early D1 (Trupchun phase) thrusting at or near the surface is documented in sediments of the Err nappe by olistoliths derived from the overriding Julier-Bernina thrust sheets in Late Aptian to Middle Turonian (110–90 Ma) "Couches Rouges" (Chanels Formation of FURRER et al., 1985; see Figs 2 and 3 in FINGER, 1978) and by Late Cretaceous God-Drosa flysch of at least Cenomanian to Middle Turonian (< 88–97 Ma) age (RÖSLI, 1945; FURRER et al., 1985). Incipient thrusting is not as well documented in the Margna, Platta and Lizun-Forno units due to the absence of dated flysch, but the youngest sediments in these units (Aptian-Albian Emmat Formation of FURRER et al., 1985; Neocomschiefer of STÖCKLIN, 1949; DIETRICH, 1970) place a maximum age limit (100–115 Ma) on the cessation of quiet, pelagic to hemipelagic sedimentation. This break in sedimentation may be related to the onset of subduction. The 76–89 Ma S1 white mica age range presented above indicates that parts of the imbricated Mesozoic sequence in the Err nappe attained depths compatible with high P/T greenschist facies mylonitization and isoclinal folding no later than 20 Ma after the onset of thrusting at the surface (Fig. 10c). An age range of 80 to 88 Ma for D1 greenschist facies metamorphism is more realistic given the lack of structural evidence for a temporal overlap of D1 and D2 deformations.

The P-T paths inferred for the Margna and Err nappes (Fig. 10) suggest that the Margna nappe, and with it the Platta ophiolites, attained somewhat greater depths during D1 than did the Err nappe. Based on arguments advanced in the previous section, the P-T path for Platta nappe is assumed to approximate that for the Margna nappe. If one assumes an average mid-crustal density of 2.7 g/cm$^3$, the minimum pressures of 800–900 MPa derived above for D1 greenschist facies deformation in the southern part of the Err nappe correspond to burial depths of 21 to 25 km (Fig. 10c). Considered together with the average D1 temperature of about 300 °C in the Err nappe, this depth range represents a geotherm of about 15 °C/km. Another interesting aspect of this D1 burial depth is that the implied thickness of the units overlying the Err-Corvatsch nappe far exceeded the current thickness (ca. 5 km) of the Julier-Bernina nappe. This suggests the formation during D1 of an upper crustal nappe pile, possibly consisting of Upper Austroalpine units (labelled UAA in Fig. 10c) that either slid off to the east during D2 extension (Fig. 10d), or that were eroded sometime during Late Cretaceous to middle Tertiary time. The former hypothesis calls for the accommodation of large D2 extensional displacement in the roof of the Julier-Bernina nappe and/or in other overlying units. D2 tectonites at the base of the Upper Austroalpine Languard nappe (Fig. 1) may be a manifestation of such extension (see structural data in Fig. 15b of FROITZHEIM et al., 1994), but the amount of D2 displacement along this contact has yet to be ascertained.

The 69–73 Ma syn-D2 amphibole ages and 67–80 Ma syn-D2 white mica ages and in this study indicate that D2 low-angle normal faulting (Ducan-Ela phase) followed D1 subduction and nappe stacking by only a few million years (Fig. 10d). The coincidence of top-to-the-E normal faulting with decreased pressure during D2 suggests that large tracts of the sutured Lower Austroalpine and Liguro-Piemontese oceanic crust were pulled up and out from under the D1 nappe pile already in Late Cretaceous time. Based on the distribution of D2 deformation northwest (HANDY, 1996) and southeast of the Engadine line (MÜLLER, 1982; FROITZHEIM et al., 1994), most of this D2 extensional uplift was accommodated in the Err-Corvatsch nappe. The amount of this extensional uplift is roughly constrained by the difference in pressure estimates obtained above from D1 and D2 white mica-bearing assemblages. The D2-induced pressure drop at 300–350 °C is bracketed at between 400 MPa and 600 MPa, corresponding to about 11 to 16 km of vertical uplift. If one accepts these values and the burial depths cited above for D1 to be realistic, then the geothermal gradient can be inferred to have in-

creased to 30–40 °C/km during the D2 event. D2 extension probably did not continue much beyond 60 to 65 Ma, the age range of the stratigraphically highest clastic sediments in late orogenic, Gosau extensional basins of Upper Austroalpine units to the north and east (RATSCHBACHER et al., 1989 and references therein).

High P/T metamorphism also affected Penninic units deeper within the Tertiary nappe pile (i.e., west of the Turba mylonite zone in Fig. 1), as evidenced by glaucophane and crossite in the Upper Penninic Avers Bündnerschiefer (OBERHÄNSLI, 1977, 1986), the wide distribution of 3T white mica polytypes in Middle Penninic units (FREY et al., 1983), and the occurrence of eclogite in the Lower Penninic Adula nappe (e.g., HEINRICH, 1986). We tentatively correlate the blue amphiboles in the Avers Bündnerschiefer with the syn- to post-D1 and/or D2 Na-amphiboles of the Platta nappe examined in this study, but hasten to add that the age of the other high P/T relics in the Middle and Lower Penninic units is still unclear and may well be younger than the blue amphiboles dated in this study. The Adula eclogites, for example, are probably early Tertiary age, based on stratigraphic and structural arguments recently reviewed in FROITZHEIM et al. (1996) and Early Tertiary radiometric ages (GEBAUER et al., 1992; BECKER, 1993). In the Suretta, Schams and Tambo nappes, most traces of high P/T metamorphism are overprinted by penetrative, amphibolite to greenschist facies deformation (Ferrera phase of MILNES and SCHMUTZ, 1978; D1 of SCHREURS, 1993; BAUDIN et al., 1993). Syn-tectonic mica and amphibole ages constrain this deformation to have occurred some 30 to 50 Ma ago (SCHREURS, 1993 and references therein). Thus, subduction and accretion of the Middle Penninic units to the already sutured Apulian-Tethyan margin (not shown as a separate stage in Fig. 10) probably post-date the 67–100 Ma time bracket for D1 and D2 events in the Err and Platta nappes, but predate the onset of amphibolite facies, Ferrera phase deformation and metamorphism in the Schams, Suretta and Tambo nappes some 50 Ma ago.

Lower anchizonal D3 (Blaisun phase) deformation accommodated N–S to NNE–SSW directed shortening in the Err-Corvatsch, Platta, and Margna nappes and pre-dates both the Bergell intrusion and Turba mylonitic shearing (LINIGER and NIEVERGELT, 1990; LINIGER, 1992). D3 deformation is therefore inferred to be broadly coeval with Schams-D1 (Ferrera phase) and the early stages of Schams-D2 backflow (Niemet phase of MILNES and SCHMUTZ, 1978) under amphibolite to greenschist facies conditions in the Schams and Suretta nappes (Figs. 10e, 10f). Ferrera phase deformation in the Schams area is kinematically related to the N-directed thrusting that transported the previously sutured Lower Austroalpine and Liguro-Piemontese units (LINIGER and NIEVERGELT, 1990) about 50 to 75 km onto the Paleocene-Eocene Arblatsch flysch (Fig. 10e; e.g., MILNES, 1978). The actual thrust surface accommodating this displacement must have been located at or just within the base of the Lizun-Forno and Platta ophiolites (marked x in Fig. 10e), but is no longer exposed, presumably due to faulting out during subsequent Turba mylonitization (Fig. 10f). The P-T path of the Err-Corvatsch, Platta and Margna units in the hangingwall of this thrust is poorly constrained for the Early Tertiary interval between D2 and D3, but the mineral equilibria discussed in the previous section support a retrograde path involving decompression and cooling (Fig. 10). This suggests that the sutured Austroalpine and Upper Penninic units underwent uplift roughly at the same time as the Middle Penninic units below experienced high P/T metamorphism and as the Paleocene-Eocene Arblatsch flysch and other Lower Penninic flysch units were deposited in front of the advancing Alpine orogen.

The high-angle normal faults depicted in figures 2 and 3 are partly related to top-to-the-E D4 shearing along the low-angle, Turba mylonite zone in mid-Tertiary time (Turba phase of FROITZHEIM et al., 1994) and partly to mid- to late Tertiary faulting along the Engadine line (HANDY, 1996). The Turba mylonite zone excised at least 2 km of Penninic material and emplaced a cold hangingwall containing the Lower Autroalpine-Penninic suture against a hot footwall comprising the Middle Penninic Schams, Suretta and Tambo nappes and the Upper Penninic Avers Bündnerschiefer (NIEVERGELT et al., 1996). As LINIGER and NIEVERGELT (1990) note, this extension is responsible for the marked contrast in the style and metamorphic conditions of early to mid-Tertiary deformation on either side of the Turba mylonite zone.

Sub-anchizonal D5 folds (Domleschg phase of FROITZHEIM et al., 1994) in the Err-Corvatsch, Platta, and Margna nappes were not analyzed in this study (see HANDY, 1996), but deform the Turba mylonite zone (LINIGER and NIEVERGELT, 1990) and are also recognized in the Schams area (D3 of SCHREURS, 1993). These folds accommodated NNW–SSE directed shortening and are probably associated with uplift of the Bergell intrusive body (ROSENBERG et al., 1995) and of the southern part of the Suretta nappe (Fig. 10g; LINIGER, 1992).

We conclude by pointing out that the evidence for Late Cretaceous subduction, nappe accretion and subsequent extensional uplift refutes Hsü's (1995) hypothesis of convergent offscraping within a subduction zone mélange as a mechanism for imbricating and exhuming the Margna and Platta nappes. While mélange structure in the sense of Hsü (1968) is indeed observed locally on the outcrop scale (Ring et al., 1989; Dürr, 1992), there is no evidence for such structure on map scales of 1: 5,000 or greater, at least along the Err-Platta boundary (e.g., Tietz, 1993; Klahr, 1994). Extensive mapping and structural analysis in recent years along this contact (Liniger, 1992; Handy et al., 1993; Froitzheim et al., 1994; Handy, 1996) reveal that, despite the structural complexity associated with polyphase deformation, D1 thrust sheets are coherent and contain a recognizable Mesozoic stratigraphy. Although mylonitized, they certainly do not form chaotic, randomly oriented bodies that are diagnostic of classical mélanges (e.g., the Franciscan mélanges; see Hsü, 1971). We therefore propose that the exhumation of the sutured Margna, Platta, and Err-Corvatsch nappes involved a more complicated, multi-stage unroofing history including Late Cretaceous east-west extension (D2, Ducan-Ela phase), early Tertiary northward thrusting (D3, Blaisun phase), and early to mid-Tertiary normal faulting (Turba phase) above the rising Lepontine dome. More studies that combine structural geology with phase petrology and radiometric dating are necessary to affirm or modify this idea.

**Acknowledgements**

The mineral ages and geobarometric data, as well as many of the figures in this paper were presented already in 1992 and 1993 in Poster and Abstract form at Swiss Tectonics Meetings in Lausanne and Zürich. Publication of these results was delayed by the first author's move to the University of Giessen in 1994. We have enjoyed discussions and field trips with many colleagues during this project, but would especially like to thank Ivan Mercolli and Tjerk Peters for their continued interest in our work. The Diploma mapping of Christian Regli, Christoph Mattenberger and Urs Klahr contributed significantly to the development of our ideas. We also thank F. Zweili and A. Werthemann (Bern) for preparing the photomicrographs on such short notice. The manuscript benefited from the reviews of R. Gieré, R. Oberhänsli, and D. Vance, as well as from the careful critique of R. Ferreiro Mählmann and the comments of M. Frey. The financial support of the Swiss National Science Foundation in the form of project grant 2971-088 and Profil-2 grant 21-30598.91, both to MRH, is acknowledged with gratitude. The Isotope Geology Laboratory was supported by SNF grant 20-40442.94.

**References**

Baudin, T., Marquer, D. and Persoz, F. (1993): Basement-cover relationships in the Tambo nappe (Central Alps, Switzerland): geometry, structure and kinematics. J. Struct. Geol., 15, 543–553.

Becker, H. (1993): Garnet peridotite and eclogite Sm–Nd mineral ages from the Lepontine dome (Swiss Alps) – new evidence for an Eocene high pressure metamorphism in the Central Alps. Geology, 21, 599–602.

Bernoulli, D., Bertotti, G. and Froitzheim, N. (1990): Mesozoic Faults and Associated Sediments in the Austro-Alpine – South Alpine Passive Continental Margin. Mem. Soc. Geol. It., 45, 25–38.

Blanckenburg, F.v. and Villa, I.M. (1988): Argon retentivity and excess Ar in hornblendes from garben-schists of the Western Tauern Window, Eastern Alps. Contr. Miner. Petrol. 100, 1–11.

Bousquet, R., Goffé, B., Henry, P., Le Pichon, X. and Chopin, C. (in press): Kinematic, Thermal and Petrological Model of the Central Alps: Lepontine Metamorphism in the Upper Crust and Eclogitisation of the Lower Crust. Tectonophysics.

Cornelius, H.P. (1932): Geologische Karte der Err-Julier-Gruppe 1:25'000. Schweiz. Geol. Kommission, Spezialkarte Nr. 115A.

Cornelius, H.P. (1950): Geologie der Err-Julier-Gruppe: Der Gebirgsbau. Beitr. Geol. Karte Schweiz [N.F.] 70/2.

Deutsch, A. (1983): Datierung an Alkaliamphibolen und Stilpnomelan aus der südlichen Platta-Decke. Eclogae geol. Helv. 76, 295–308.

Dietrich, V. (1970): Die Stratigraphie der Platta-Decke. Eclogae geol. Helv. 63, 631–671.

Dürr, S.B. (1992): Structural history of the Arosa Zone between Platta and Err Nappes east of Marmorera (Grisons): Multi-Phase deformation at the Penninic-Austroalpine Plate boundary. Eclogae geol. Helv. 85, 361–374.

Eberli, G.P. (1988): The evolution of the southern continental margin of the Jurassic Tethys Ocean as recorded in the Allgäu Formation of the Austroalpine Nappes of Graubünden (Switzerland). Eclogae geol. Helv., 81, 175–214.

England, Ph. and Molnar, P. (1990): Surface uplift, uplift of rocks, and exhumation of rocks. Geology, 18, 1173–1177.

Evans, B.W. and Patrick, B.E. (1987): Phengite-3T in high-pressure metamorphosed granitic orthogneisses, Seward Peninsula, Alaska. Can. Mineral., 25, 141–158.

Ferreiro Mählmann, R. (1995): Das Diagenese-Metamorphose-Muster von Vitrinitreflexion und Illit-"Kristallinität" in Mittelbünden und im Oberhalbstein. Teil 1: Bezüge zur Stockwerktektonik. Schweiz. Mineral. Petrogr. Mitt., 75/1, 85–122.

Ferreiro Mählmann, R. (1996): Das Diagenese-Metamorphose-Muster von Vitrinitreflexion und Illit-"Kristallinität" in Mittelbünden und im Oberhalbstein. Teil 2: Korrelation kohlenpetrographischer und mineralogischer Parameter. Schweiz. Mineral. Petrogr. Mitt., 76, 23–46.

Finger, W. (1978): Die Zone von Samaden (Unterostalpine Decken, Graubünden) und ihre jurassischen Brekzien. Mitt. Geol. Inst. ETH und Univ. Zürich, N.F. 224: 1–140.

Flisch, M. (1982): Potassium-Argon Analysis, 151–158 in: G.S. Odin (editor), Numerical dating in stratigraphy. Wiley & Sons, New York.

Frey, M., Hunziker, J.C., Frank, W., Bocquet, J., Dal

PIAZ, G.V., JÄGER, E. and NIGGLI, E. (1974): Alpine metamorphism of the Alps. A review. Schweiz. Mineral. Petrogr. Mitt., 54, 247–290.

FREY, M., HUNZIKER, J.C., JÄGER, E. and STERN, W.B. (1983): Regional Distribution of White K-Mica Polymorphs and their Phengite Content in the Central Alps. Contr. Mineral. Petrol., 83, 185–197.

FROITZHEIM, N. (1992): Formation of recumbent folds during synorogenic crustal extension (Austroalpine Nappes, Switzerland). Geology, 20, 923–926.

FROITZHEIM, N. and EBERLI, G.P. (1990): Extensional detachment faulting in the evolution of a Tethys passive continental margin, Eastern Alps, Switzerland. Geol. Soc. Am. Bull., 102, 1297–1308.

FROITZHEIM, N., SCHMID, S.M. and CONTI, P. (1994): Repeated change from crustal shortening to orogen-parallel extension in the Austroalpine units of Graubünden. Eclogae geol. Helv., 87/2, 559–612.

FROITZHEIM, N., SCHMID, S.M. and FREY, M. (1996): Mesozoic paleogeography and the timing of eclogite-facies metamorphism in the Alps: A working hypothesis. Eclogae geol. Helv., 89/1, 81–110.

FURRER, H., AEMISSEGGER, B., EBERLI, G., EICHENBERGER, U., FRANK, S., NAEF, H. and TRÜMPY, R. (1985): Field workshop on Triassic and Jurassic sediments in the Eastern Alps of Switzerland. Mitt. Geol. Inst. ETH und Univ. Zürich, N.F. 248, 1–81.

GEBAUER, D., GRÜNENFELDER, M., TILTON, G., TROMMSDORFF, V. and SCHMID, S. (1992): The geodynamic evolution of garnet-peridotites, garnet-pyroxenites and eclogites of Alpe Arami and Cima di Gagnone (Central Alps) from Early Proterozoic to Oligocene. Schweiz. Mineral. Petrogr. Mitt., 72, 107–111.

GUNTLI, P. and LINIGER, M. (1989): Metamorphose in der Margna-Decke im Bereich Piz da la Margna und Piz Fedoz (Oberengadin). Schweiz. Mineral. Petrogr. Mitt., 69/2, 289–302.

HAMMERSCHMIDT, K. and FRANK, E. (1991): Relics of high pressure metamorphism in the Lepontine Alps (Switzerland) – $^{40}Ar/^{39}Ar$ and microprobe analyses on white micas. Schweiz. Mineral. Petrogr. Mitt., 71, 261–274.

HANDY, M.R., HERWEGH, M. and REGLI, C. (1993): Tektonische Entwicklung der westlichen Zone von Samedan (Oberhalbstein, Graubünden, Schweiz). Eclogae geol. Helv., 86/3, 785–817.

HANDY, M.R. (1996): The Transition from Passive to Active Margin Tectonics: A Case Study from the Zone of Samedan (Eastern Switzerland). Geol. Rund.

HEINRICH, C.A. (1986): Eclogite facies regional metamorphism of hydrous mafic rocks in the Central Alpine Adula nappe. J. Petrol., 27, 123–154.

HERWEGH, M. (1992): Kinematik der Julierüberschiebung am Südwestrand der Zone von Samedan (Unterostalpin, Julierpass). Unpubl. Lizentiatsarbeit, Univ. Bern, 133 pp.

HUNZIKER, J.C., FREY, M., CLAUER, N., DALLMEYER, R.D., FRIEDRICHSEN, H., FLEHMIG, W., HOCHSTRASSER, K., ROGGWILER, P. and SCHWANDER, H. (1986): The evolution of illite to muscovite: Mineralogical and isotope data from the Glarus Alps, Switzerland. Contrib. Min. Petr., 92, 157–180.

HSÜ, K.J. (1968): Principles of melanges and their bearing on the Franciscan-Knoxville paradox. Geol. Soc. Am. Bull., 80, 927–953.

HSÜ, K.J. (1971): Franciscan melanges as a model for eugeosynclinal sedimentation and underthrusting tectonics. J. Geophys. Res., 76, 1172–1180.

HSÜ, K.J. (1995): The Geology of Switzerland: An Introduction to Tectonic Facies. Princeton University Press, 250 pp.

KLAHR, U. (1994): Strukturgeologische Untersuchungen des penninisch-unterostalpinen Grenzbereiches im Raume Grevasalvas (Graubünden). Unpubl. Lizentiatsarbeit, Univ. of Bern, 115 pp.

KRETZ, R. (1983): Symbols for rock-forming minerals. Am. Mineral., 68, 277–279.

LI, S., WANG, S., CHEN, Y., LIU, D., QIU, J., ZHOU, H. and ZHANG, Z. (1994): Excess argon in phengite from eclogite: Evidence from dating of eclogite minerals by Sm–Nd, Rb–Sr, and $^{40}Ar/^{39}Ar$ methods. Chem. Geol., 112, 343–350.

LINIGER, M. (1992): Der Ostalpin-Penninische Grenzbereich im Gebiet der nördlichen Margna-Decke (Graubünden, Schweiz). Ph. D. Thesis, ETH-Zürich, 186 pp.

LINIGER, M. and GUNTLI, P. (1988): Bau und Geschichte des zentralen Teils der Margna-Decke. Schweiz. Mineral. Petrogr. Mitt., 70, 41–54.

LINIGER, M. and NIEVERGELT, P. (1990): Stockwerk-Tektonik im südlichen Graubünden. Schweiz. Mineral. Petrogr. Mitt., 70, 95–101.

MASSONNE, H.-J. and SCHREYER, W. (1987): Phengite geobarometry based on the limiting assemblage with K-feldspar, phlogopite, and quartz. Contrib. Mineral. Petrol., 97, 147–155.

MATTENBERGER, C. (1994): Strukturelle Untersuchungen im unterostalpin-penninischen Grenzbereich (Oberengadin, Graubünden). Unpubl. Lizentiatsarbeit, Univ. of Bern, 175 pp.

MILNES, A.G. (1978): Structural Zones and Continental Collision, Central Alps. Tectonophysics, 47, 369–392.

MILNES, A.G. and SCHMUTZ, H. (1978): Structure and history of the Suretta nappe (Pennine zone, Central Alps), a field study. Eclogae geol. Helv., 71, 19–33.

MISCH, P. (1969): Paracrystalline Microboudinage of Zoned Grains and other Criteria for Synkinematic Growth of Metamorphic Minerals. Am. J. Sci., 267, 43–46.

MÜLLER, D. (1982): Geologie und Petrographie der Bernina-I.-Kristallisation, Deformation und Geochemie des südlichen Corvatschgranits im Oberengadin GR. Unpubl. Diplomarbeit, ETH-Zürich.

NIEVERGELT, P., LINIGER, M., FROITZHEIM, N. and FERREIRO MÄHLMANN, R. (1996): Early Tertiary crustal extension in the Central Alps: The Turba Mylonite Zone (Eastern Switzerland). Tectonics, 15, 329–340.

OBERHÄNSLI, R. (1977): Chemische Untersuchungen an Glaukophan-führenden basischen Gesteinen aus den Bündnerschiefern Graubündens. Schweiz. Mineral. Petrogr. Mitt., 58, 139–156.

OBERHÄNSLI, R. (1986): Blue amphiboles in metamorphosed mafic rocks from the Central Alps. Geol. Soc. Am. Mem., 164, 239–247.

PHILLIPP, R. (1982): Geologie und Petrographie der Bernina-Decke: Grevasalvas-Lunghin. Unpubl. Diplomarbeit, ETH-Zürich.

RATSCHBACHER, L., FRISCH, W., NEUBAUER, F., SCHMID, S.M. and NEUGEBAUER, J. (1989): Extension in compressional orogenic belts: The eastern Alps. Geology, 17, 404–407.

REGLI, CH. (1992): Strukturgeologische Untersuchungen am Westrand der Zone von Samedan (Unterostalpine Decken, Julierpass). Unpubl. Lizentiatsarbeit, Univ. of Bern, 99 pp.

RING, U., RATSCHBACHER, L., FRISCH, W., BIEHLER, D. and KRALIK, M. (1989): Kinematics of the Alpine plate-margin: structural styles, strain and motion along the Penninic-Austroalpine boundary in the Swiss Alps. J. Geol. Soc. London, 146, 835–849.

ROSENBERG, C.L., BERGER, A. and SCHMID, S.M. (1995): Observations from the floor of a granitoid pluton:

Inferences on the driving force of final emplacement. Geology, 23, 5, 443–446.

RÖSLI, F. (1945): Sedimentäre Zone von Samaden. Eclogae geol. Helv., 37/2, 355–383.

SCHMID, S.M. and FROITZHEIM, N. (1993): Oblique slip and block rotation along the Engadine line. Eclogae geol. Helv., 86/2, 569–593.

SCHREURS, G. (1993): Structural analysis of the Schams nappes and adjacent tectonic units: implications for the orogenic evolution of the Pennine zone in eastern Switzerland. Bull. géol. France, 164, 415–435.

SPILLMANN, P. (1993): Die Geologie des penninisch-ostalpinen Grenzbereichs im südlichen Berninagebirge. Ph. D. Thesis, ETH-Zürich, 262 pp.

SPRY, A. (1969): Metamorphic Textures. Pergamon Press, Oxford, 350 pp.

STAUB, R. (1948): Über den Bau der Gebirge zwischen Samaden und Julierpass und seine Beziehungen zum Falknis-Berninaraum. Beitr. Geol. Karte Schweiz [N.F.] 93.

STÖCKLIN, J. (1949): Zur Geologie der nördlichen Errgruppe zwischen Val d'Err und Weissenstein (Graubünden). Unpubl. Ph. D. Thesis, ETH-Zürich, 105 pp.

TIETZ, R. (1993): Strukturgeologische Untersuchungen an der Grenze Unterostalpin-Penninikum im Raume Piz Lunghin und Piz dal Sasc (Graubünden). Unpubl. Diplomarbeit, Univ. Bern, 129 pp.

TONARINI, S., VILLA, I.M., OBERLI, F., MEIER, M., SPENCER, D.A., POGNANTE, U. and RAMSAY, J.G. (1993): Eocene age of eclogite metamorphism in Pakistan Himalaya: Implications for India-Eurasia collision. Terra Nova, 5, 13–20.

TROMMSDORFF, V. (1983): Petrologic aspects of serpentine metamorphism. Rendiconti Soc. It. Mineral. Petrol., 38, 549–559.

TROMMSDORFF, V. and NIEVERGELT, P. (1983): The Bregaglia (Bergell) Iorio intrusive and its field relations. Mem. Soc. Geol. It., 26, 55–68.

TROMMSDORFF, V, PICCARDO, G.B. and MONTRASIO, A. (1993): From magmatism through metamorphism to sea floor emplacement of subcontinental Adria lithosphere during pre-Alpine rifting (Malenco, Italy). Schweiz. Mineral. Petrogr. Mitt., 73, 191–203.

TRÜMPY, R. (1975): Penninic-Austroalpine boundary in the Swiss Alps: A presumed former continental margin and its problems. Amer. J. Sci., 279, 209–238.

Manuscript received April 3, 1996; revised manuscript accepted September 16, 1996.